Arabian Journal of Geosciences (2018) 11:32
https://doi.org/10.1007/s12517-017-3368-3

ORIGINAL PAPER

Geological and geophysical investigations to delineate the subsurface extension and the geological setting of Al Ji'lani layered intrusion and its mineralization potentiality, Ad Dawadimi District, Kingdom of Saudi Arabia

E. K. El-Sawy[1,2] · A. Eldougdoug[3] · M. Gobashy[4]

Received: 25 January 2017 / Accepted: 26 December 2017

Abstract

In the present study, Al Ji'lani layered intrusion was subjected to integrated field, petrographic, processing of ASTER data, and geophysical investigations to delineate its subsurface extension and to determine the chronological order of the exposed rocks. The intrusion is surrounded by foliated granodiorite and both were intruded by younger granite. Processing of ASTER data revealed that the intrusion incorporated foliated granodiorite masses along its NE corner indicating its younger age (postorogenic) setting contrary to what have been proposed by previous authors. Also, this is further confirmed by the presence of an offshoot from the intrusion in the South-East corner as well as freshness and undeformed nature of the gabbroic rocks. Petrographically, the gabbroic rocks are characterized by the presence of kelyphytic coronas around olivine in contact with plagioclase, magnetite-orthopyroxene symplectites after olivine, and symplectites between plagioclase and magnetite/ilmenite. These textures are explained in terms of interaction with late deuteric magmatic fluids and not to metamorphism as believed before. The extensive geophysical analyses of the Al Ji'lani prospect using aeromagnetic data suggest complicated combination of magnetic bodies composed mainly of gabbroic rocks intruding the foliated granodiorite with variable magnetic susceptibilities. Gradient analysis, tilt angle and edge detection techniques extracted the shallow subsurface magnetic boundaries and a probable multiple bodies in the subsurface are detected. The 3-dimensional constraint inversion using parametrized trust region algorithm revealed the deep subsurface distribution of magnetic susceptibilities of the bodies. Two resolved bodies are clear, a northern more shallow body, and a southern, deeper and laterally extend to the south and southwest. The calculated volume from the inverted model representing the Al Ji'lani layered intrusion is approximately 518.7 km^3 as calculated to 6.0 km depth. The body could be extended to a deeper depth if a different proposed model geometry is adjusted. The surface area of the exposed body is only 42.39 km^2. Several magnetic anomalies are defined within the intrusion and are considered potential sites of mineralization. The south east corner of the gabbroic intrusion is traversed by a shear zone trending ENE-WSW which hosts sulfide-bearing quartz veins with high silver content (Samrah Prospect) associated with an offshoot from the layered gabbro. The shear zone should be followed to the west where the intrusion extends for a distance of about 10 km in the subsurface to the southwest of the exposed part of the intrusion.

Keywords Al Ji'lani · Ad Dawadimi · Layered intrusion · Magnetic anomalies · Principal components analysis (PCA)

✉ E. K. El-Sawy
elsawykamal@gmail.com

1 Geoexploration Techniques Department, Faculty of Earth Sciences, King Abdulaziz University, P.O. Box 80206, Jeddah 21589, Kingdom of Saudi Arabia

2 Geology Department, Faculty of Science, Al-Azhar University (Assiut branch), Assiut, Egypt

3 Geology Department, Faculty of Science, Cairo University, Giza, Egypt

4 Geophysics Department, Faculty of Science, Cairo University, Giza, Egypt

Introduction

The Arabian Shield covers an area over 650,000 Km^2 in western and southwestern parts of the Arabian Peninsula and covers about 25% of the area of Saudi Arabia. It extends 2000 Km from north to south and 700 Km at its widest point from east to west, and contains one of the largest and best exposed assemblages of Neoproterozoic (1000–750 Ma) rocks in the world. The Arabian Shield is bounded to the east and south by successions of Phanerozoic sedimentary rocks and Red Sea rift separated the Nubian and Arabian Shields. The Arabian Shield consists of volcano-sedimentary successions with plutonic complexes that have been deformed, metamorphosed and intruded by numerous, predominantly younger granitic plutons.

Since the mid of the 1970s, there is a general agreement that the greater part of the Arabian Shield was developed from oceanic crustal material in a sequence of island arcs during the period 900–640 Ma (Al Shanti and Mitchell 1976; Frisch and Al Shanti 1977; Fleck et al. 1980; Bokhari and Kramers 1981; Stacey and Stoeser 1983; and Jackson 1985), but debate continues concerning the extent to which older (Early Proterozoic or Archean) continental crust was involved. Several studied (Schmidt et al. 1973; Stacey et al. 1980; Stacey and Hedge 1984; Calvez et al. 1983) show involvement of older (Archean) continental crust along the eastern margin of the Arabian Shield, which occurs under the Phanerozoic successions along the eastern margin of the shield as evident from geological studies.

Two main types of evolutionary models of the Arabian Shield have been suggested:

1-The development and accretion of ensiamatic island arcs (Al Shanti and Mitchell 1976; Bakor et al. 1976; Greenwood et al. 1976; Frisch and Al Shanti 1977; Gass 1977; Gass and Smewing 1981;Schmidt et al. 1973; and Stoeser and Camp 1984.

2-Tectonic modification by arc magmatism and/or rifting of an older sialic basement (Garson and Shalaby 1976; Delfour 1981; and Kemp et al. 1982).

Although arc accretion appears to have been a major shield-forming process for the Arabian-Nubian Shield, the concept of microplate accretion may also be applicable for the Arabian part of the shield (Kroner 1985; Vail 1983; Stoeser and Camp 1984; Johnson 1999; Genna et al. 2002; Johnson et al. 2011).

Stoeser and Camp (1984) proposed a microplate accretion model for the Pan-African evolution of the Arabian Shield which consists of five terranes that are separated by four or five ophiolitic-bearing suture zones. The western part of the shield is composed of at least three intraoceanic island arc terranes (Asir, Higaz, Midyan), whereas the eastern part contains two terranes (Afif and Rayn) of continental affinity (Fig. 1). Stoeser and Camp (1984) and others proposed that the evolution of the Arabian Shield could be divided into five main phases: 1—Rifting of the African craton (1200–950 Ma). 2—Ensiamatic island arcs development (950–715 Ma). 3—Formation of the Arabian-Nubian Neocraton by microplate accretion and continental collision (715–640 Ma). 4—Collision-related intracratonic magmatism and tectonism (640–550 Ma); and 5—Epicontinental subsidence (550 Ma).

Johnson (1999) and Johnson et al. (2011) presented a terrane model for the evolution of the Arabian Shield. It is developed through processes of crustal accretion spanning about 300 Ma that started with the creation of juvenile oceanic basins and ended with the creation of 45 Km thick continental crust. Most of the exposed rocks of the Arabian Shield are between 870 and 550 Ma old, although some materials as much as 2000 Ma old are present. The older materials contain zircon grains, which were eroded from old continental crust and incorporated as detrital grains in younger sedimentary and inherited zircon crystal in plutonic rocks and rare intact Paleoproterozoic rocks.

The processes of arc accretion, amalgamation and suturing, the deposition of post-amalgamation assemblages, and intrusion of granitoid and subordinate gabbroic rocks were followed by the most prominent structural feature of the Arabian Shield; the northwest trending major left-lateral wrench Najd fault system (630–550 Ma) that has as much as 200–300 Km of displacement.

Within the framework of the evolutionary plate-tectonic model of the Arabian Shield, mafic plutonites can be grouped into syntectonic subduction related (island arcs) calc-alkaline metagabbro-diorite complexes, and post-tectonic intrusive gabbros. A similar classification has been adopted for the Egypt Nubian Shield (Takla et al. 1981; Hassan and Hashad 1990; and Akaad 1996). The first group is regionally metamorphosed up to the greenschist facies and is known as the older metagabbros. The second group is mostly fresh and unmetamorphosed and is known as the younger gabbros. These younger gabbros are widely distributed in the Saudi Arabian Shield particularly the eastern part of the shield (Fig. 1). Also, these younger gabbros were described from Yemen Arabian Shield (Abdel Wahed et al. 2006, Egypt Nubian Shield (El Ramly and Hermina 1978a and b), and Sudan Nubian Shield (Tawfik 1981). The metagabbros are Cryogenian (~850–780 Ma), while the younger gabbros are Ediacaran 620~) -590 Ma) (Coleman et al. 1972 and Cloeman et al. 1977; Johnson and Kattan 2012; Surour Adel et al. 2016).

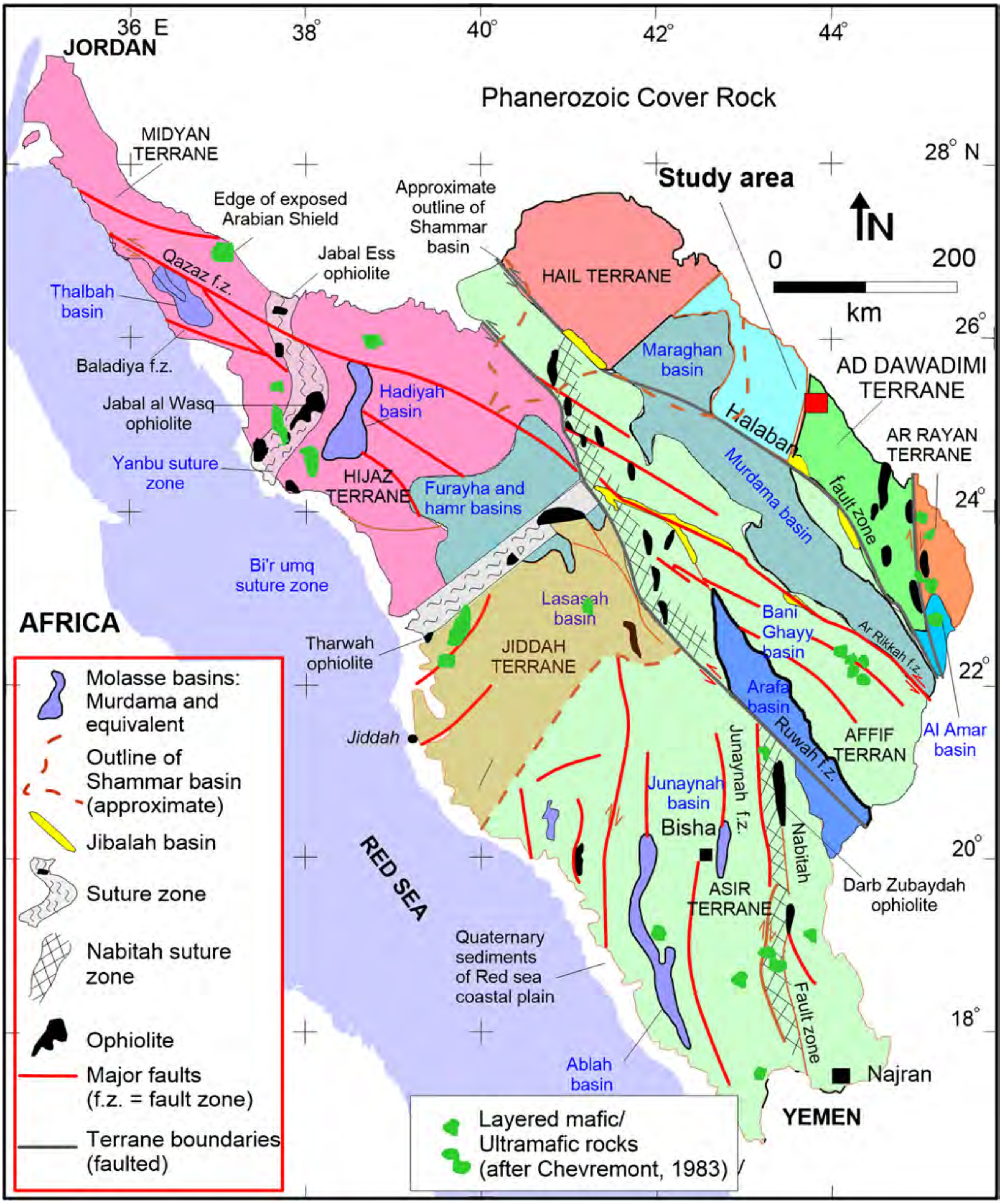

Fig. 1 Simplified geologic sketch map of the Arabian Shield (from Nehlig et al. 2002) showing the terranes and their boundaries, and the main Pan-African structural features and sedimentary basins. Major fault zones, such as Ruwah, Ar Rikah, Halaban, and Qazaz, belong to the Najd fault system

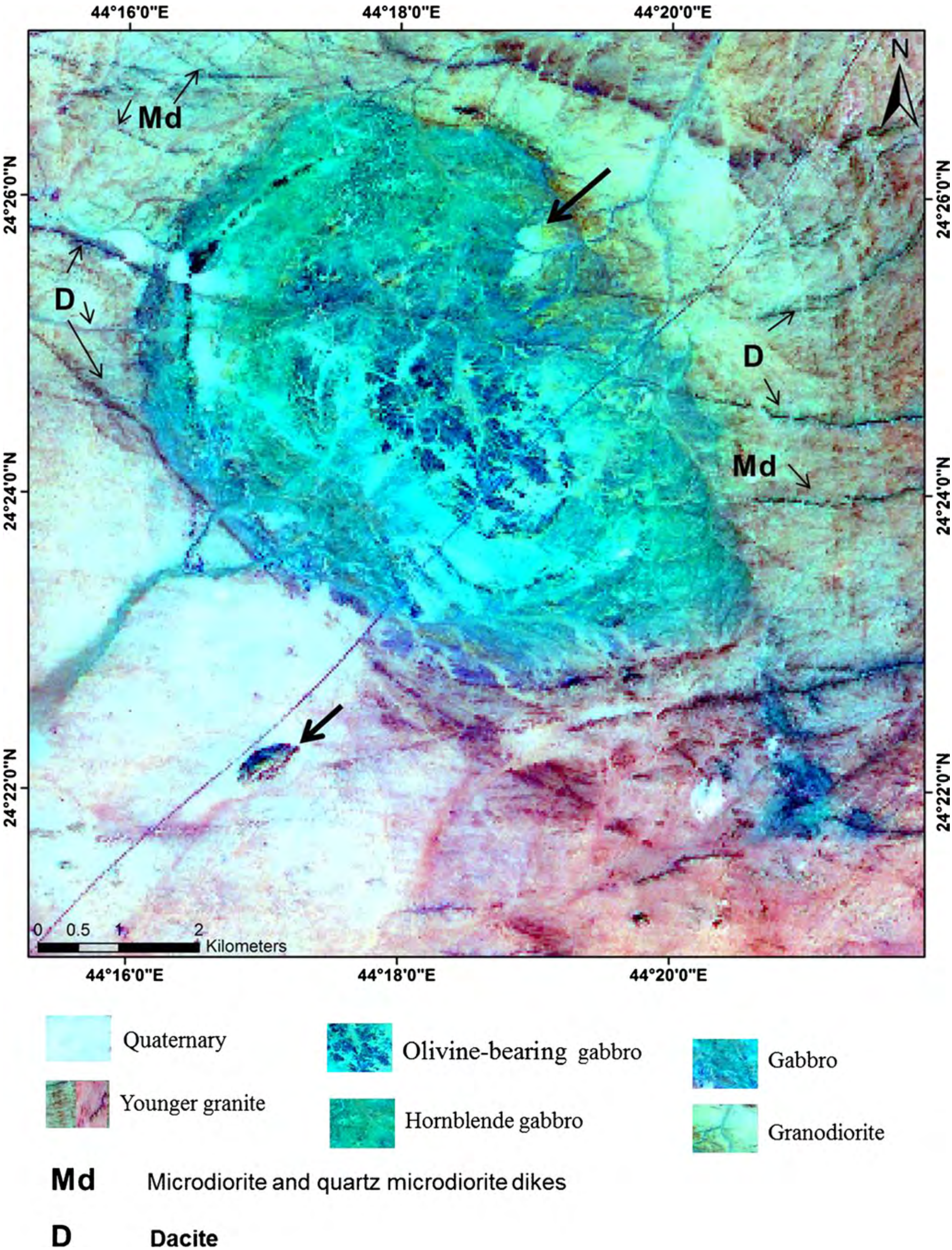

Fig. 2 Principal component analysis image (PC1:PC2:PC3 in RGB) of Al Ji'lani layered intrusion

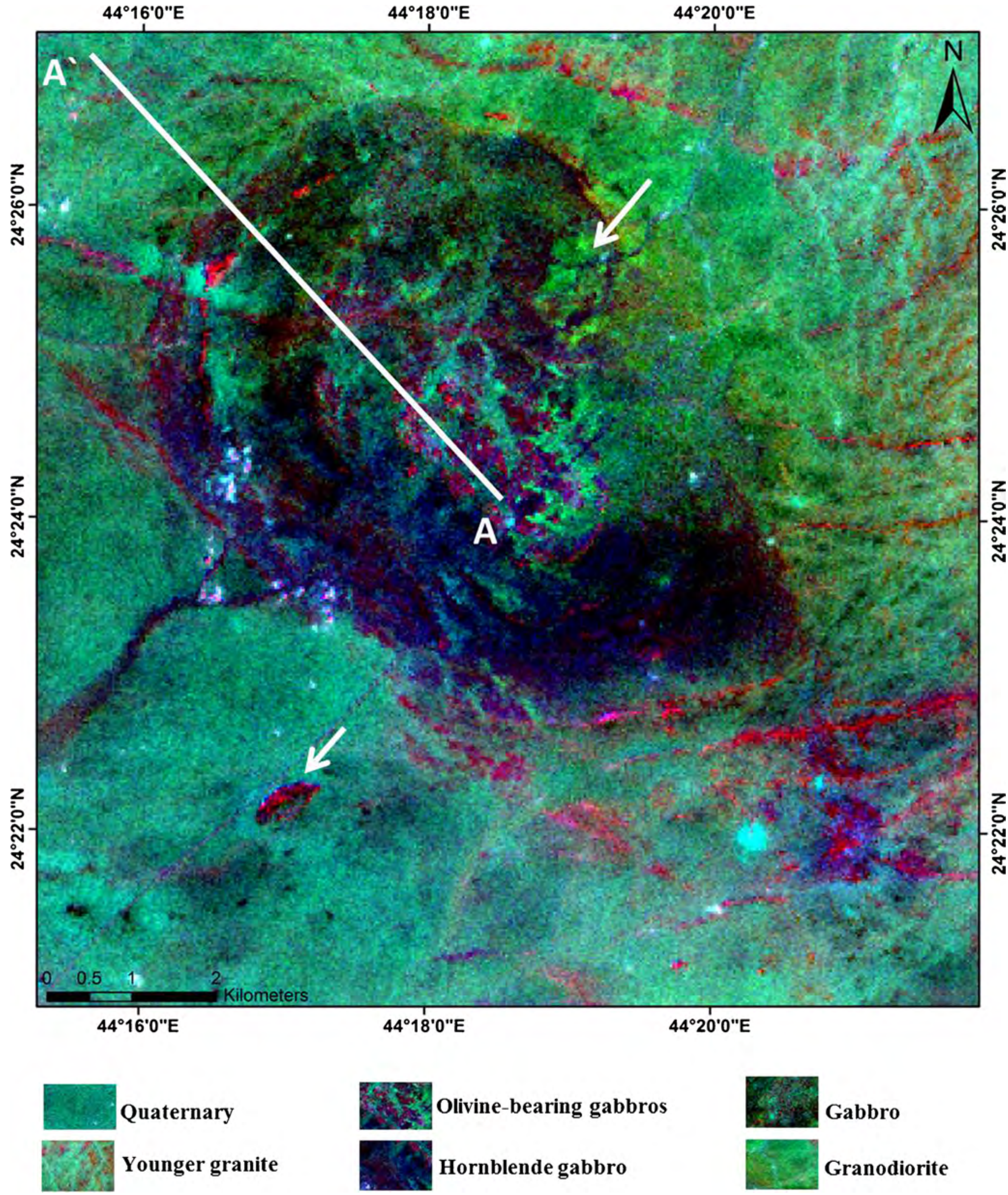

Fig. 3 Band ratios image 4/1:4/5:4/7in RGB of Al Ji'lani layered intrusion

Each of the above mentioned mafic plutonites hosts certain type(s) of mineralization(s). Rare or uncommon Fe–Ti (magnetite and ilmenite) mineralization is associated with the metagabbro-diorite complexes (Takla et al. 1981). The

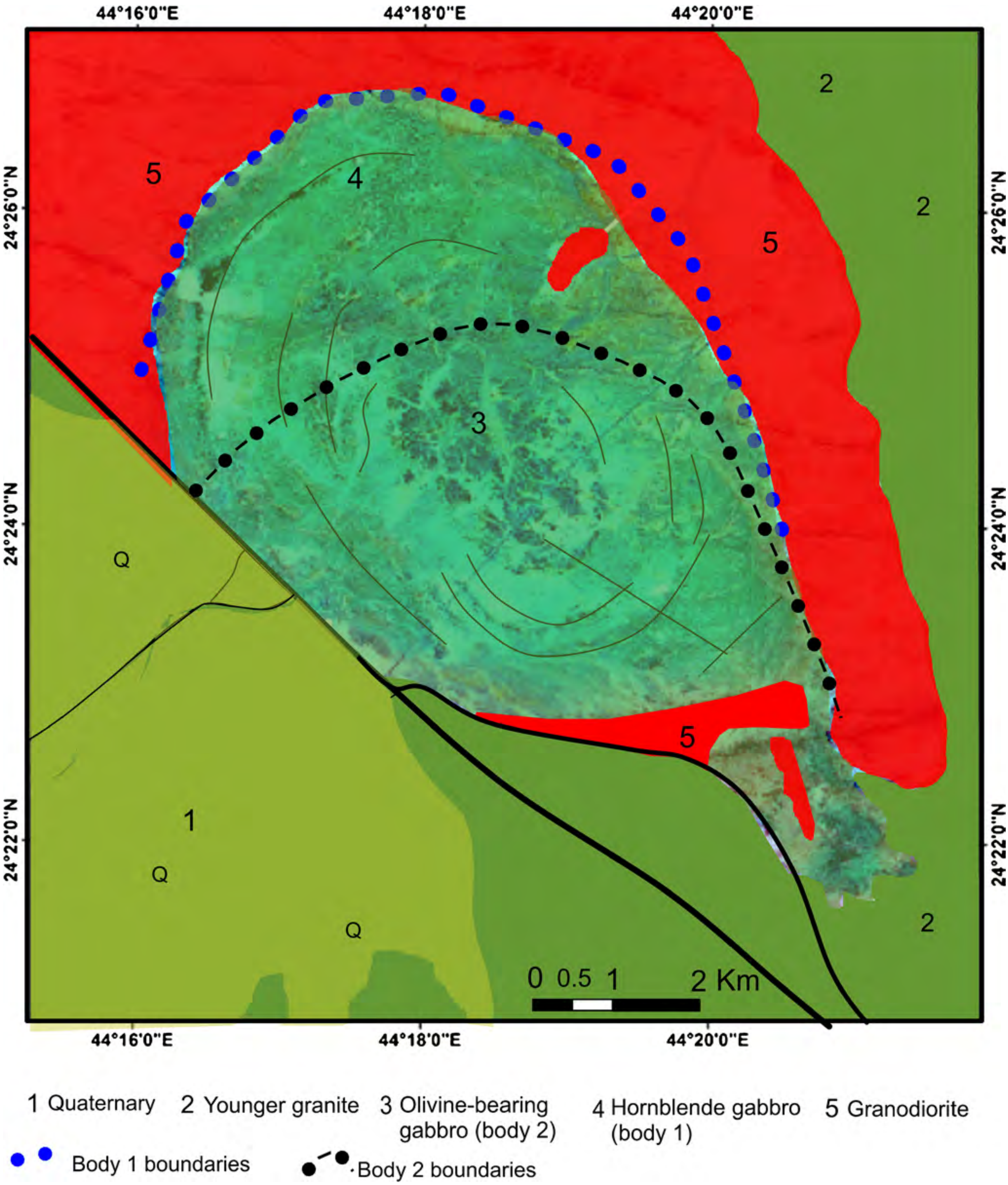

Fig. 4 Geological map of Al Ji'lani layered intrusion (modified after Delfour et al. 1982)

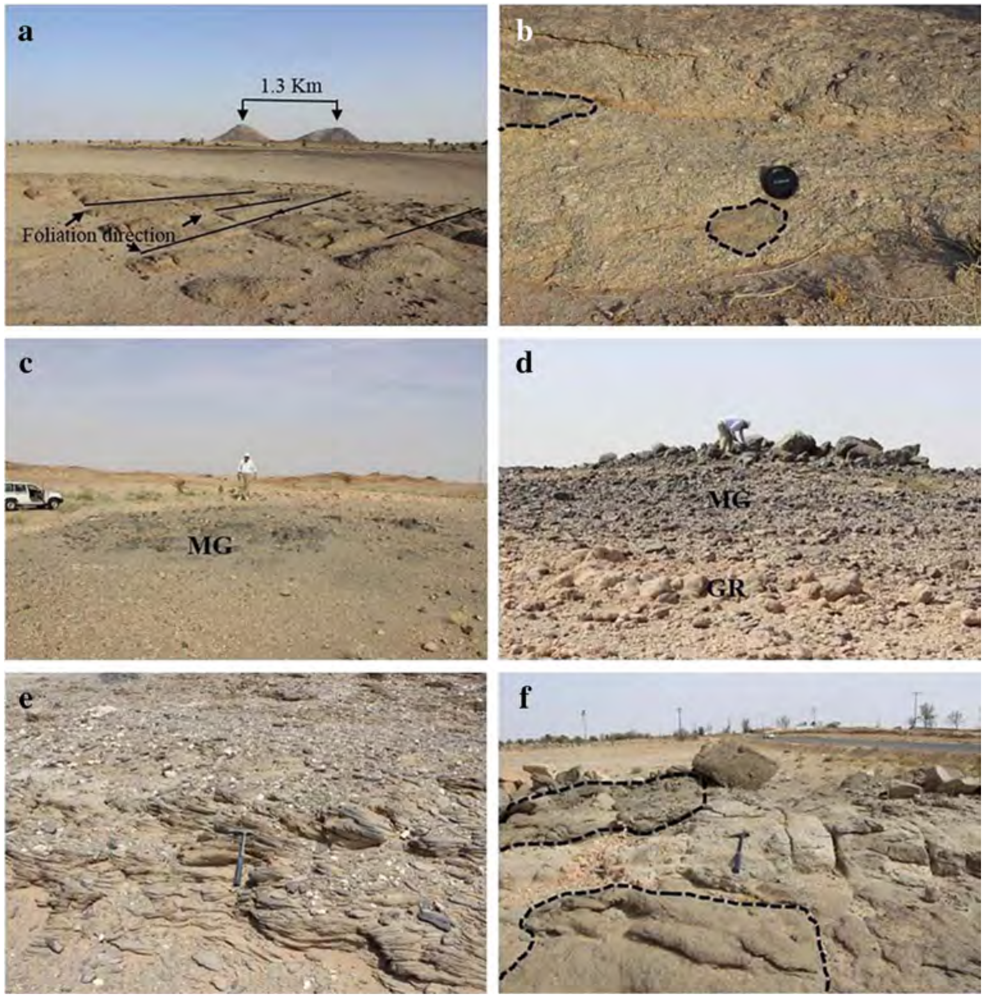

Fig. 5 **a** Foliated granodiorite, NW of Al Ji'lani layered intrusion (JLI). **b** Rock fragments in the foliated grandiorite, NW of the JLI. **c** A metagabbro fragment (MG) enclosed in granodiorite, eastern side of the JLI. **d** Sharp contact between metagabbro (MG)and the granodiorite(GR), eastern side of the JLI. **e** Schist fragments enclosed in the granodiorite, eastern side of the JLI, and **f** Amphibolite fragments enclosed in the granodiorite, eastern side of the JLI

younger gabbros host the following types of mineralizations: (1) Cu-Ni sulfide deposits in layered mafic-ultramafic intrusions, e.g. Gabbro Akarm (Hussein 1990 and Helmy and Mogessie 2001); Cu-Ni mineralization associated with the central gabbroic unit of Khamal gabbro- anorthite complex, NW Saudi Arabia (Harbi et al. 2006). (2) Fe-Ti-(P) oxide deposits, e.g. Abu Ghalaga Fe-Ti (Hussein 1990), nelsonite, the magnetite- ilmenite-apatite ore, associated with hornblende gabbro at Kolminab, south Eastern Desert, Egypt (Basta and Girgis 1969), and nelsonite ore associated the central gabbronorite of Wadi Khamal gabbro-anorthosite complex, NW Saudi Arabia (Harbi et al. 2006). (3) Gold-bearing quartz veins at the contact between the younger gabbros and felsic intrusions, e.g. Umm Rus mine, Central Eastern Desert, Egypt (Hussein 1990; El Tokhi and El Muslem 2002), Um Eleiga, South Eastern Desert, Egypt (Takla et al. 1990), Um Tenedba, South Eastern Desert, Egypt (Takla et al. 1997), Zalm mine, Central Saudi Arabia, where gold-bearing quartz veins are hosted by fresh gabbro intruded by granite (Harbi et al. 2003; Harbi 2004).

The present study deals with one of the well exposed layered gabbroic intrusion in Ad Dawadimi terrane in the northeastern corner of the Arabian Shield (Al Ji'lani intrusion) in order to determine its geologic setting. Previous studies (e.g. Theobold 1966; Al Shanti 1974; Delfour et al. 1982) described it as a synorogenic intrusion. From the mineral exploration point of view, it is very important to define the tectonic setting, whether it is synorogenic or postorogenic, since the latter hosts numerous types of mineralization's.

To better understand the geologic setting of the Al Ji'lani layered intrusion, field, remote sensing, and petrographic studies were conducted and integrated with

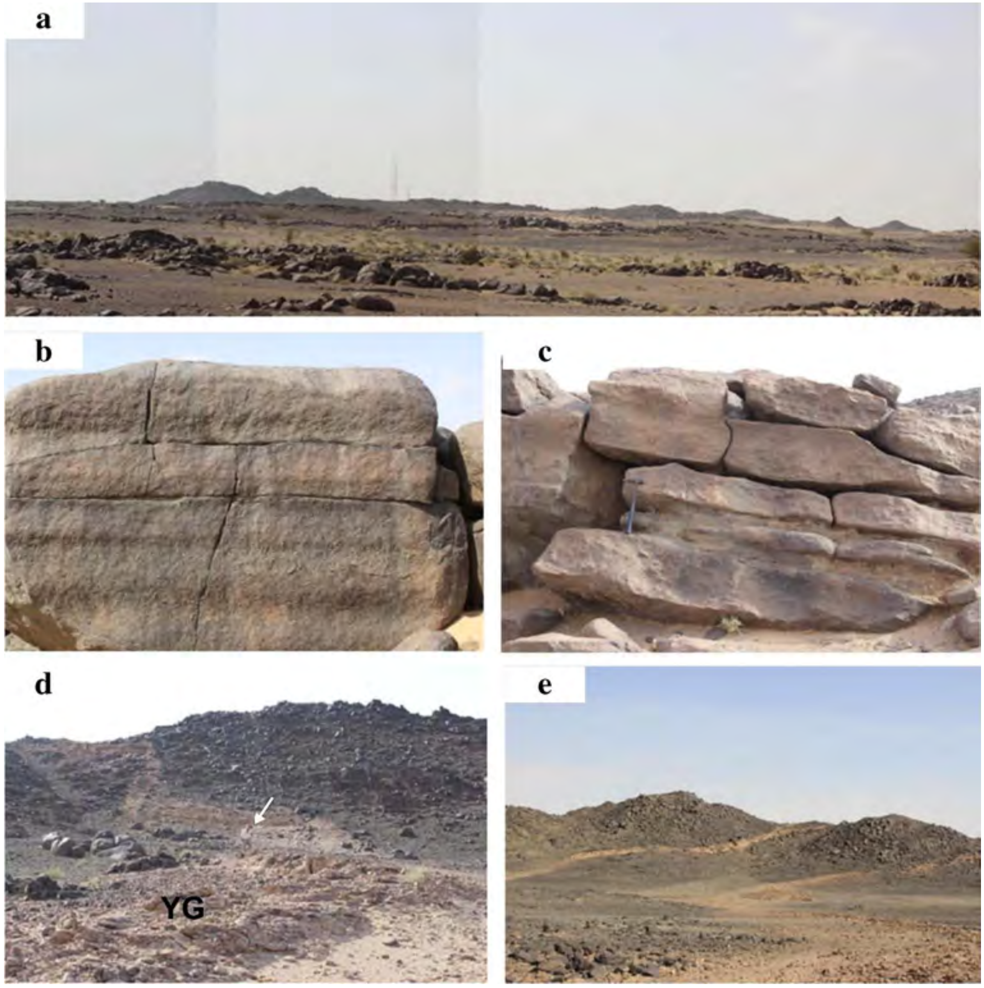

Fig. 6 **a** A panorama showing layering in the JLI, Photo looking north (Photo width ~ 3 km). **b** Nearly horizontal microbands in the JLI, Photo looking north (Photo width ~ 3.5 m). **c** Slightly dipping microbands in the JLI, Photo looking north. **d** Younger granite intruding the JLI, southern side of the intrusion, Photo looking north (Photo width ~ 40 m). **e** A younger microgranite granite dyke (3 m wide) traversing the JLI, southern side of the intrusion, Photo looking north

intensive joint processing results from the available aeromagnetic data and magnetic susceptibilities measured from collected rock samples over and around the target body data. Gradients and up-to-date regularization techniques are implemented in the geophysical study.

Geological studies

Processing of ASTER data

The Al Ji'lani layered gabbroic intrusion is surrounded by granodiorite and both were intruded by younger granitic rocks. Theobold (1966) mapped the intrusion as mostly olivine gabbro and ortho- and clinopyroexene gabbros interlayered with amphibolites derived from the metamorphism of the mafic rocks. Al Shanti (1974) stated that the Al Ji'lani mafic intrusion was emplaced into older metasediments and both were subsequently intruded by granitic rocks. These felsic rocks have incorporated numerous fragments of the country and have also disrupted the eastern and southeastern margins of the intrusion. Delfour et al. (1982) mentioned that the Ad Dawadimi granitic rocks enclose various types of inclusions such as schist and Al Ji'lani layered gabbro.

The Advanced Spaceborne Thermal Emission and Reflection Radiometer (ASTER) instrument has fourteen spectral bands three in the visible and near-infrared (VNIR), six in the short-wave-infrared (SWIR) and five in the thermal infrared (TIR) with 15 m, 30 m and 90 m spatial resolution respectively. Two image processing techniques Principal Component Analysis (PCA) and band combination have been applied on the ASTER data for discrimination and lithological mapping of the rock units exposed in the study area (Sabins 1997; Chen 2000; Rowan and Mars 2003; Rowan et al. 2003;

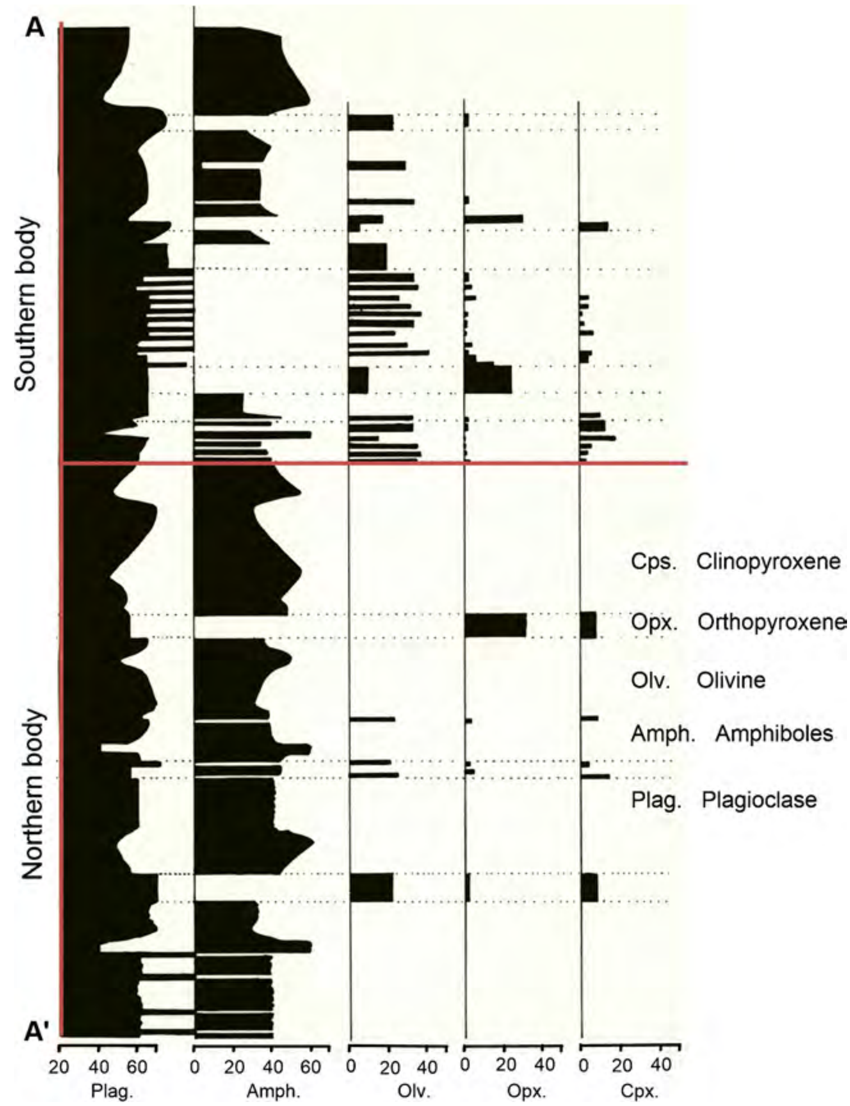

Fig. 7 The variation of modal analyses of the rocks of Al Ji'lani layered intrusion along profile A-A` (see Fig. 3), from the periphery to the center of the intrusion (modified after Al Shanti 1974)

Gomez et al. 2005; Mars and Rowan 2006; Gad and Kusky 2007, Assiri et al. 2008; Pour and Hashim 2011 and Mouhssine et al. 2013).

Principal Component Analysis is used to produce new output bands, mostly free of noise components, and reduce of data sets the number of the new PCA output band same to the number of the input the largest percentage of data variance occur in the first PCA band and the second largest percentage of data variance occur on the second PCA band, and so on. From the output of PCA three bands (PC1, PC2, and PC3 in RGB) for better discrimination between the older granodiorite, the different gabbros of the layered intrusion (gabbro, hornblende gabbro and olivine-bearing gabbros), and younger granite (Fig. 2). The older granodiorite appears in pale blue colors, gabbro appears in deep greenish blue colors, hornblende gabbro appears in green with pale violet colors, olivine-bearing gabbros have violet colors, and younger granite has brownish red color (Fig. 2).

Band rationing is among the methods that enhance the spectral differences between bands to emphasize the differentiation and discrimination of the rock types exposed in the study area (Abrams et al. 1983, Mather 1987, and San Miguel-Ayanz and Biging 1996). By using the color composite images (RGB) with band combinations it is possible to produce new images that differentiate the rock units based on color variation. An important advantage of multispectral images is the ability to detect the important differences between exposed rock units by combining the spectral bands. By selecting particular band combination, various materials may be visually contrasted against their background by using color. It was found that the most useful band combination for discrimination of the different rock types in the area under investigation is b4/b1:b4/b5:b4/b7 as R:G:B (Fig. 3). In this image, the granodiorite shows greenish color, gabbro shows dark greenish color, hornblende gabbro shows dark violet color, olivine-bearing gabbros appear in pink color, and younger granite has greenish red color (Fig. 3).

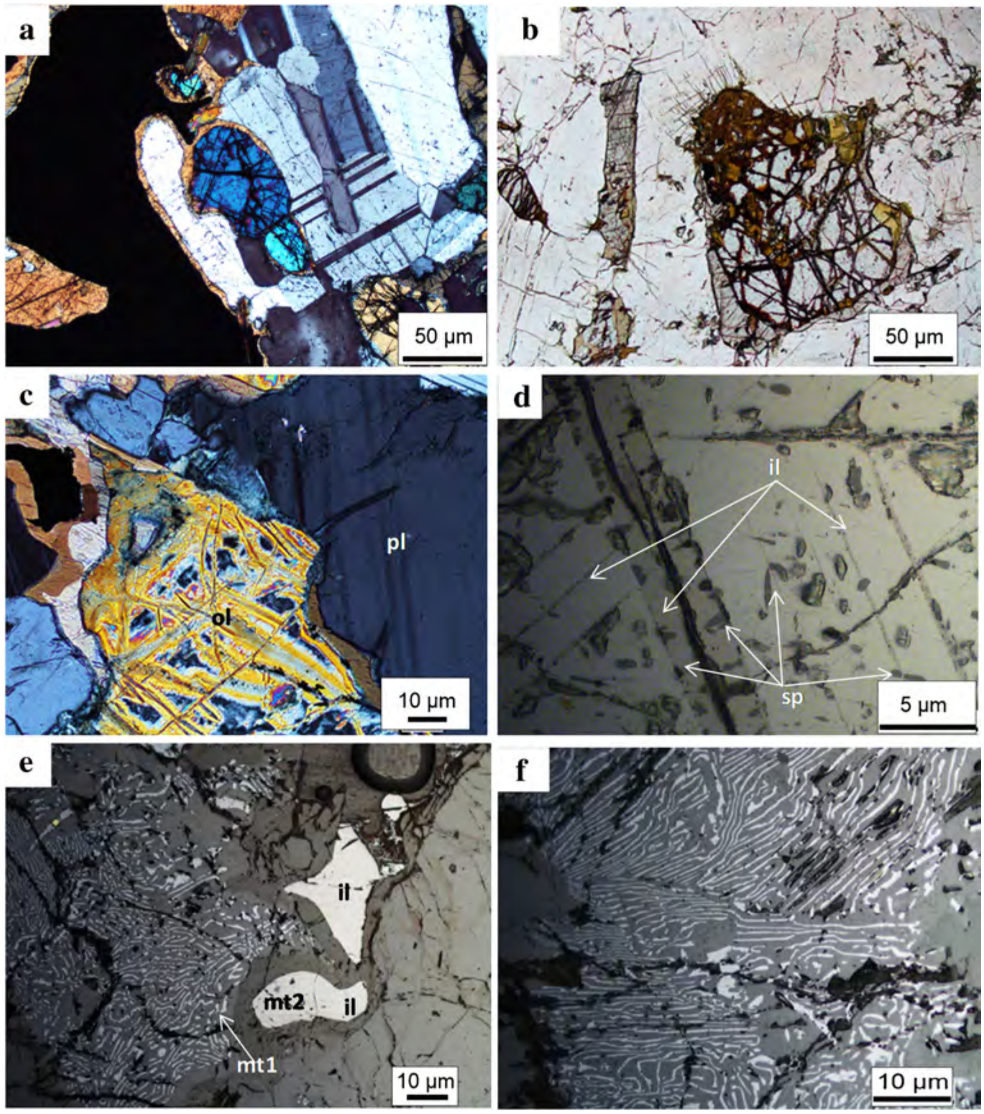

Fig. 8 **a** Cumulus olivine crystals surrounded by kelyphytic corona along contact with plagioclase (center), iron oxides surrounded by symplectite rim along contact with plagioclase (left), olivine gabbro, T.S. (Thin Section), C.N. (Crossed Nicols). **b** Cumulus olivine surrounded by kelyphytic corona along the contact with plagioclase, olivine gabbro, T.S., P.P.L. **c** Olivine altered to serpentine and surrounded by kelyphytic corona along the contact with plagioclase (pl), olivine gabbro, T.S., C.N. **d** Magnetite showing ilmenite (il) intergrowths parallel to the octahedral cleavage planes (111), spinel (sp) parallel to the cubic cleavage planes (001), and a coarse ilmenite band enclosing spinel inclusions, olivine gabbro, P.S. (Polished section), P.P.L. (Plane polarized light). **e** Symplectite intergrowths of magnetite (mt1) and orthopyrxene (MOS) after olivine and composite grains of ilmenite (il) and host rock magnetite (mt2), olivine gabbro, P.S., P.P.L. **f** Enlargement of Fig. 8e showing MOS, olivine gabbro, P.S., P.P.L.

Figures 2, 3 and 4 show that a large mass of granodiorite was enclosed at the NE corner within the Al Ji'lani layered intrusion (see the arrows in Figs. 2 and 3) indicating that the latter is younger than the foliated granodiorite. Moreover, in the SE corner of the exposed part of the intrusion a protrusion from the layered gabbro crossing the granodiorite is recognized (Figs. 2, 3 and 4). The gabbro protrusion is surrounded by and associated with younger granite, and is traversed by a shear zone trending ENE-WSW hosting sulfide (galena and sphalerite)-bearing quartz veins with high silver content (653 g/t; 5.12% Zn,1.64% Pb; Collenette and Grainger 1994). The mafic fragments enclosed in the foliated granodiorite to the east of the intrusion was mapped and identified as gabbroic rocks belonging to Al Ji'lani intrusion (Delfour et al. 1982). Field and petrographic studies show that these fragments are schists, amphibolite, and hornblebe metagabbro (possibly ophiolitic where these rocks are exposed to the east of the study area).

Accordingly, the exposed rocks in the area under investigation can be arranged from oldest to youngest as follows: 1. Granodiorite, 2. Al Ji'lani layered intrusion, and 3. Younger granitic rocks (Figs. 2, 3 and 4). The area is traversed by numerous dykes made up of microdiorite, quatz microdiorite, microgranite, dacite, and aplite, generally trending E-W and ENE-WSW (Figs. 2 and 3). The microdiorite and quatz microdiorite dykes occur along the northwestern and eastern sides outside of the intrusion traversing the granodiorite. The microgranite, dacite, and aplite dykes traverse both the

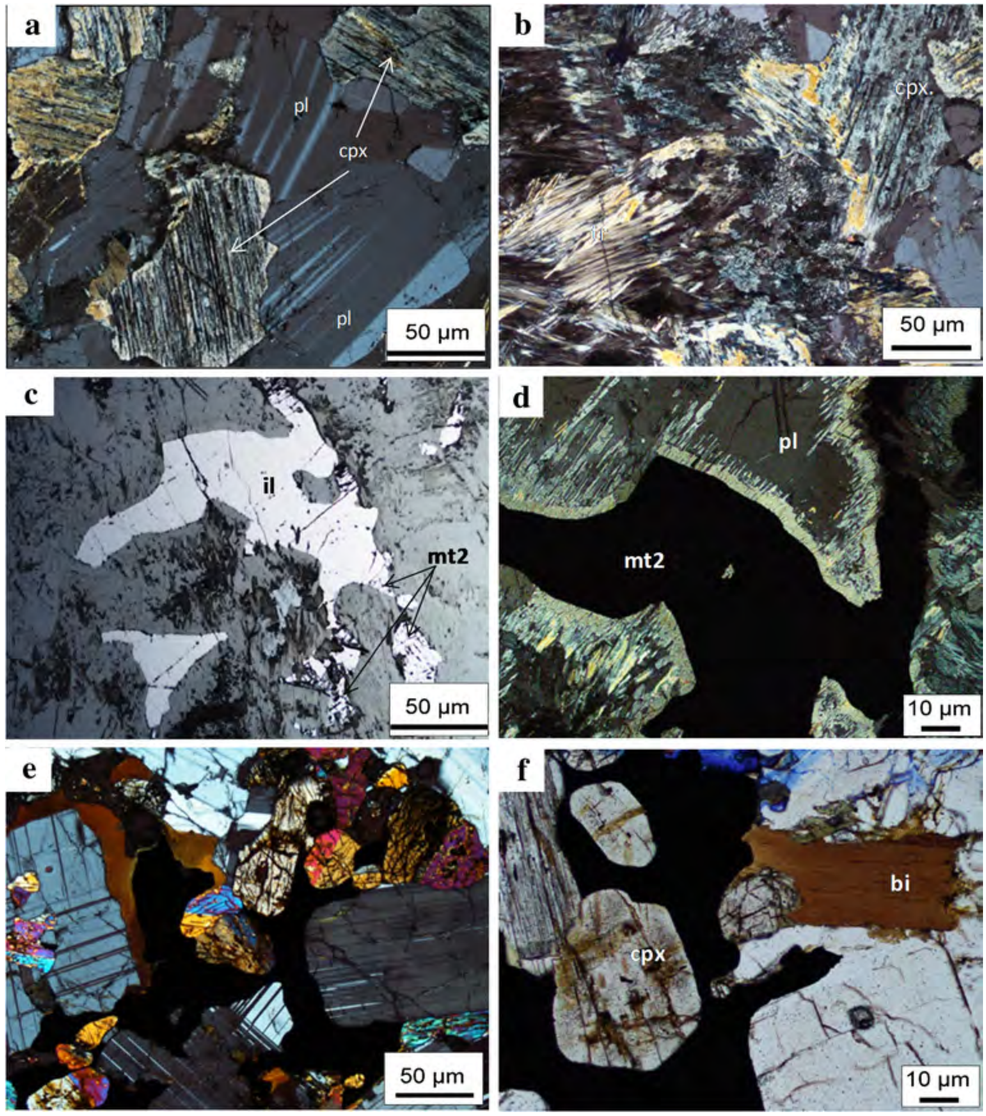

Fig. 9 **a** Intercumulus clinopyroxene to plagioclase, altered hornblende gabbro, T.S., C.N. **b** Clinopyroxene replaced by radial aggregates from tremolite, altered hornblende gabbro, T.S., C.N. **c** Composite grains of magnetite (mt2) and ilmenite (il) interstitial to silicates, altered hornblende gabbro, P.S., P.P.L. **d** Iron oxides (center) surrounded by symplectite rim from amphiboles along the contact with plagioclase (pl), plagioclase replaced by amphiboles, altered hornblende gabbro, T.S., C.N. **e** Pyroxenes and iron oxides intercumulus to plagioclase, norite, T.S., C.N. **f** Pyroxenes and iron oxides intercumulus to plagioclase with biotite flakes, (bi), olivine norite, T.S., C.N

foliated granodiorite and the layered mafic intrusion (Figs. 2, 3, 6d and e).

The granodiorite is exposed in the northwestern and eastern sides of the intrusion and is highly foliated (Fig. 5a) and contains different types of rock fragments, schist, metagabbro, and amphibolite (Fig. 5b–f). The layered intrusion is made up of interlayered fresh olivine-bearing gabbros which are more resistant to weathering and form a series of parallel ridges with the altered hornblende gabbros occupying the low lands between these ridges as they were easily weathered (Fig. 6a). The olivine-bearing gabbros are remarkably microbanded, which are nearly horizontal near the center of the intrusion (Fig. 6b) and steeply dipping outwards (Fig. 6c). The Al Ji'lani layered intrusion was intruded by the younger granite (Fig. 6d) and traversed by granitic dykes (Fig. 6e).

Petrography

The Al Ji'lani layered mafic body is a multiple intrusion and consists of northern and a southern two main bodies (See section 3). The southern intrusion consists of nearly equal proportions from olivine-bearing gabbros (olivine norite, olivine gabbro, olivine hornblende gabbro), and hornblende gabbro with some norite and gabbro norite layers. The rocks of the northern body are mainly represented by hornblende gabbro with some norite and olivine gabbro layers (Fig. 7).

The olivine gabbro consists of plagioclase, pyroxenes, hornblende, olivine, magnetite, ilmenite with disseminated fresh sulfides. Plagioclase appears to have been the earliest mineral to crystallize with associated olivine (Fig. 8a). Wherever in contact with plagioclase, olivine is surrounded

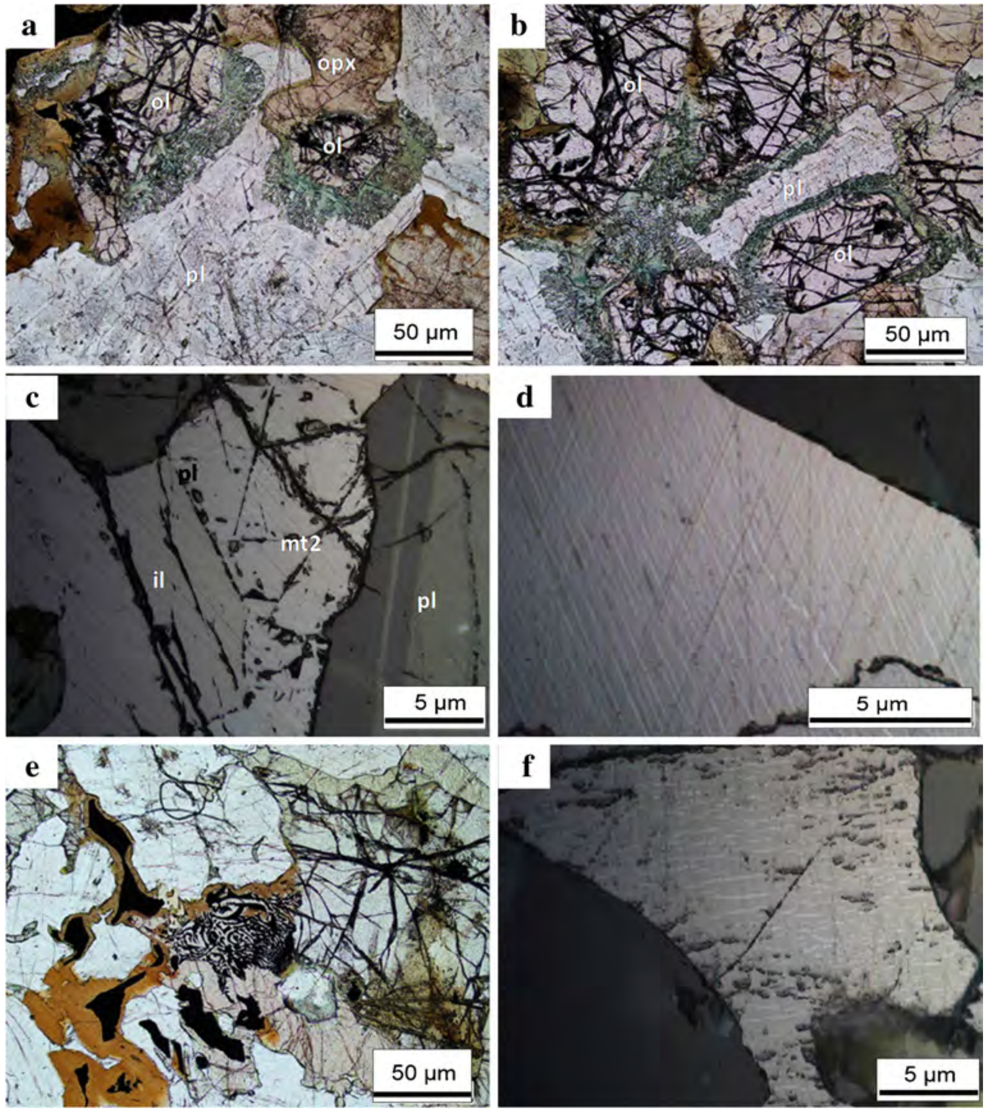

Fig. 10 **a**, **b** Cumulus olivine surrounded by kelyphytic corona along contact with plagioclase, olivine norite, T.S., P.P.L. **c** A composite aggregates of host rock magnetite (mt2) and ilmenite (il) interstitial to plagioclase, olivine norite, P.S., P.P.L. **d** Fine titanhematite lamellae oriented parallel to (0001) cleavage planes of ferriilmenite, olivine norite, P.S., P.P.L. **e** Cumulus olivine showing MOS (center), and iron oxides surrounded by symplectite rim (upper left) and biotite (bottom left), olivine gabbro, T.S., P.P.L. **f** Irregular titanhematite in ferriilmente, olivine gabbro, P.S., P.P.L

by kelyphytic coronas from orthopyroxene, and amphiboles (Fig. 8b). Primary ilmenite, magnetite, and sulfides (pyrite, pyrrhotite, and chalcopyrite) occur as interstitial composite aggregates and discrete grains between plagioclase, pyroxenes, and olivine. Olivine is sometimes altered to serpentine and is still surrounded by the kelyphytic corona (Fig. 8c). Symplectite coronas are developed between ilmenite and/or magnetite when in contact with plagioclase. The coronas are composed of amphibole and spinel (Fig. 8a). Primary magnetite contains exsolution lamellae of spinel oriented parallel to (001) cubic cleavage and ilmenite lamellae parallel to (111) octahedral cleavage (Fig. 8d). Olivine is replaced by magnetite- orthopyroxene symplectites (MOS) and rimmed by kelyphytic corona (Fig. 8e and f) these textural relations indicate that the formation of the MOS after olivine took place simultaneously with the formation of kelyphytic corona.

Similar textures have been described from different gabbroic intrusions and have been interpreted differently by different authors; late magmatic crystallization (Ambler and Ashley 1977); interaction with late deuteric fluids (Claeson 1998); high grade retrogressive metamorphism (Barton and Gaans 1988); reaction of olivine with oxygen in the solid state which was produced by the dissociation of water penetrated the hot gabbro (Efimov and Malitch 2012). These studies relied on microprobe data of the different minerals. Since the gabbros in the present study are fresh and undeformed, the interpretation of Barton and Gaans (1988) is not applicable for these rocks, and these textures can be explained in terms of the interaction with late magmatic deuteric fluids.

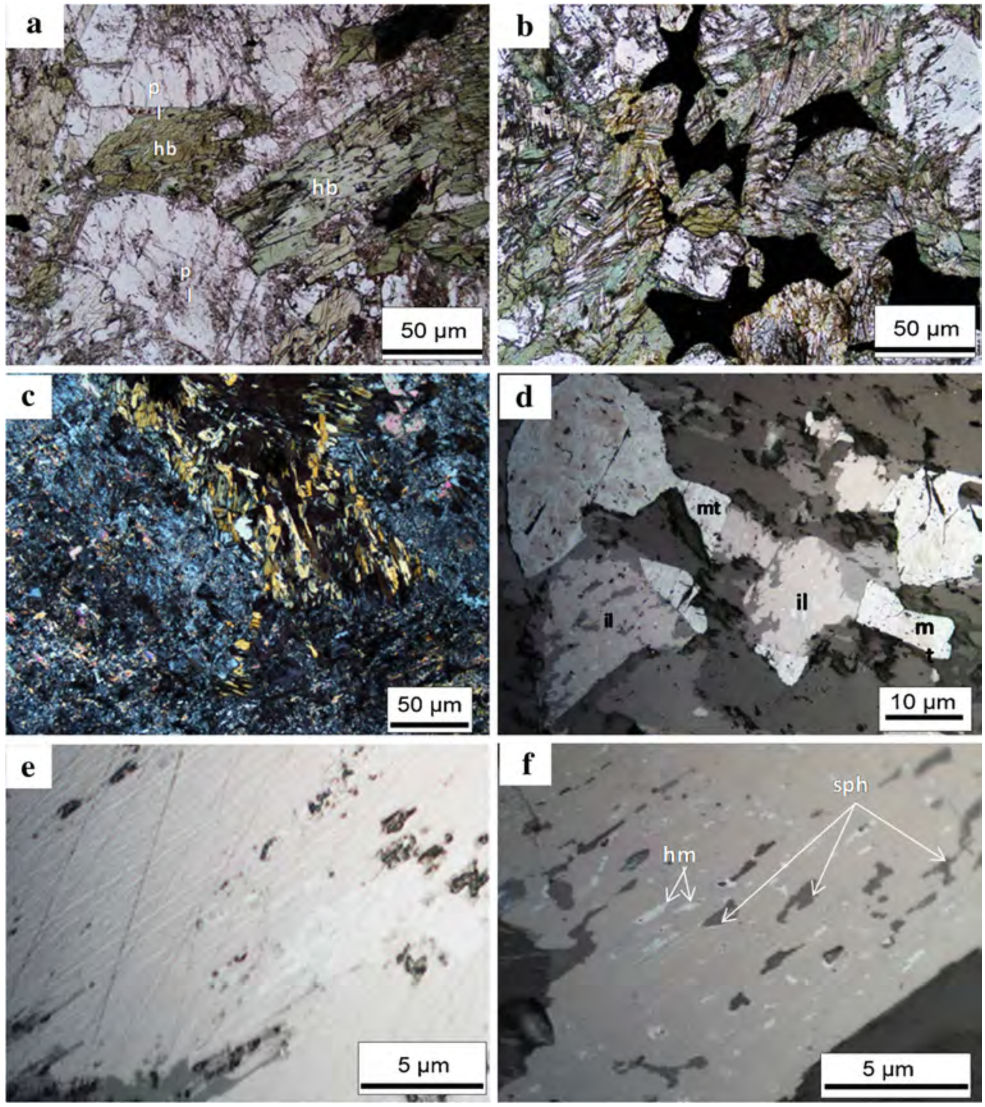

Fig. 11 **a** Intercumulus hornblende crystals, hornblende gabbro, T.S., P.P.L. **b** Intercumulus hornblende replaced by tremolite, hornblende gabbro, T.S., P.P.L. **c** Pervasive alteration of plagioclase and replacement of hornblende by tremolite, hornblende metagabbro, T.S., C.N. **d** Composite aggregates of ilmenitre (il) and magnetite (mt) interstitial to silicates, hornblende metagabbro, P.S., P.P.L. **e** Titanhematite lamellae oriented parallel to (0001) cleavage planes of ilmenite, hornblende metagabbro, P.S., P.P.L. **f** Ilmenite altered to sphene, (sph) and hematite (hm), and rutile, hornblende metagabbro, P.S., P.P.L.

In the altered hornblende gabbro, clinopyroxene crystals are intercumulus to plagioclase crystals (Fig. 9a) and are sometimes replaced by radial aggregates of tremolite (Fig. 9b). Magnetite and ilmenite occur as discrete and composite aggregates interstitial to silicates (Fig. 9c). Wherever in contact with plagioclase, the iron oxides are surrounded by symplectite rim from amphiboles (Fig. 9d). These textures indicate that these rocks were subjected to deuteric alteration by late magmatic fluids simultaneously with the olivine-bearing gabbros and not due to metamorphism as reported by Al Shanti (1974) and Theobold (1966) who described these rocks as amphibolites.

In norite and olivine norite layers near the southern margin of the southern body, pyroxenes and iron oxides are intercumulus to plagioclase with some biotite flakes (Fig. 9e and f). Olivine in contact with plagioclase is surrounded by kelyphytic coronas (Fig. 10a and b). Iron oxides (magnetite and ilmenite) are present interstitial to silicates in the form of discrete or composite aggregates (Fig. 10c). Hematite-ilmenite exsolution texture with fine hematite lamellae oriented parallel to (0001) cleavage planes of ilmenite is recorded in some of the layers (Fig. 10d). Olivine gabbro interlayered with the norite and olivine norite show olivine replaced by magnetite-orthopyroxene symplectite and the replacement of plagioclase by symplectite rim when in contact with iron oxides (Fig. 10e). Hematite-ilmenite exsolution texture with irregular hematite lamellae is also observed (Fig. 10f). Some hornblende gabbro layers are encountered and show

Fig. 12 Reduced to pole (RTP) map of the study area. The locations of the rock samples are posted on the map

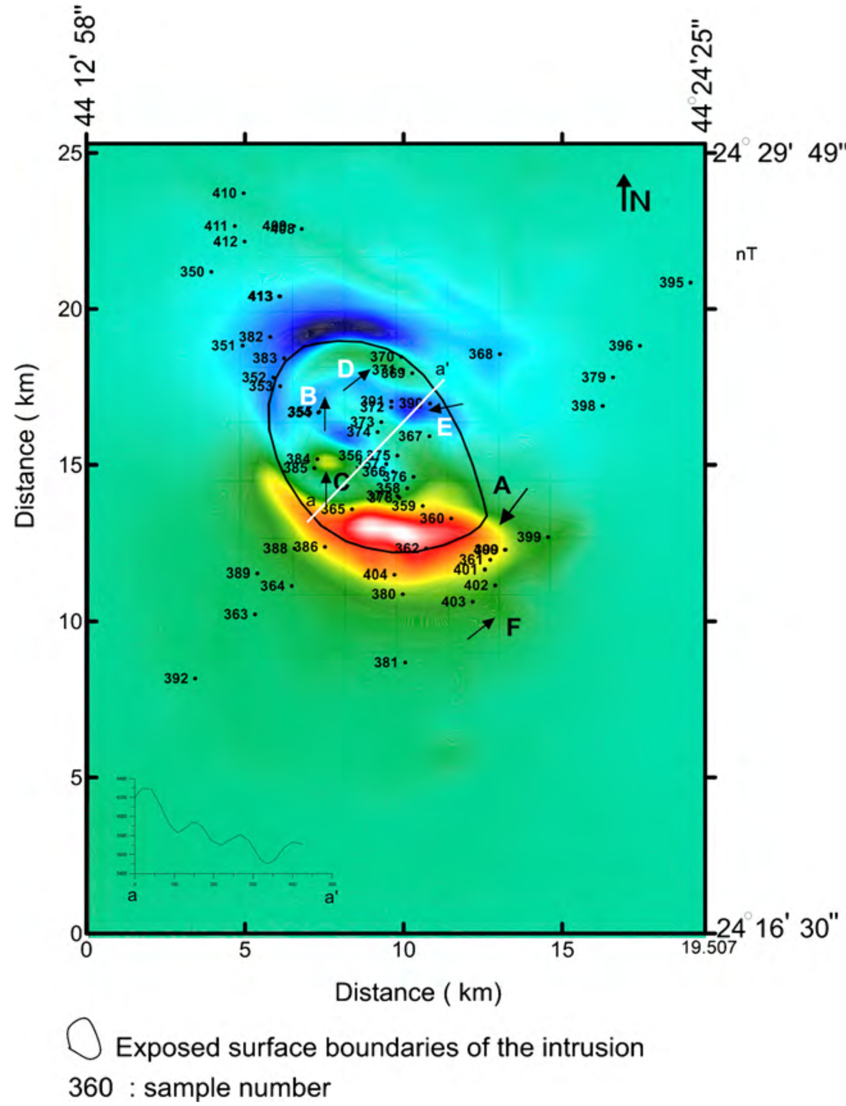

hornblende crystals intercumulus to plagioclase and partly replaced by tremolite with iron oxides occupying the interstices between the intercumulus hornblende crystals (Fig. 11a and b).

The mafic fragments enclosed within the foliated granodiorite on the eastern and southeastern sides of Al Ji'lani intrusion (See Fig. 5c) are found to be hornblende metagabbro (possibly ophiolitic where they are exposed to the east of the area) which means that the Al Ji'lani intrusion is not disrupted along its eastern margin as postulated by Al Shanti (1974). The hornblende metagabbro is pervasively altered where plagioclase is replaced by sericite and carbonate, and hornblende is replaced by temolite and chlorite (Fig. 11c). Iron oxides are present as discrete or composite aggregates from magnetite and ilmenite (Fig. 11d). Ilmenite contains hematite lamellae oriented parallel to its (0001) cleavage planes (Fig. 11e) and contrary to the hornblende gabbro described from the layered intrusion, magnetite is highly martitized and ilmenite is altered to sphene, hematite, and rutile (Fig. 11f).

Geophysical studies

Aeromagnetic data

A critical understanding of the structural and tectonic setting of a study area comes from the controlled and constraint interpretation of the available geophysical data. Integrated potential fields and modern numerical data

Table 1 Statistical analyses of the magnetic susceptibility measurements (SI units) of some collected samples from the studied area

Number of values	30
Number of missing values	0
Sum	218.008
Minimum	0.172
Maximum	31.02
Range	30.848
Mean	7.266933
Median	6.601
First quartile	3.27
Third quartile	8.687
Variance	40.96813
Average deviation	4.472391
Standard deviation	6.400635
Coefficient of variation	0.88079
Skew	30
Kurtosis	0
Critical K-S stat, alpha = .10	218.008
Critical K-S stat, alpha = .05	0.172
Critical K-S stat, alpha = .01	31.02

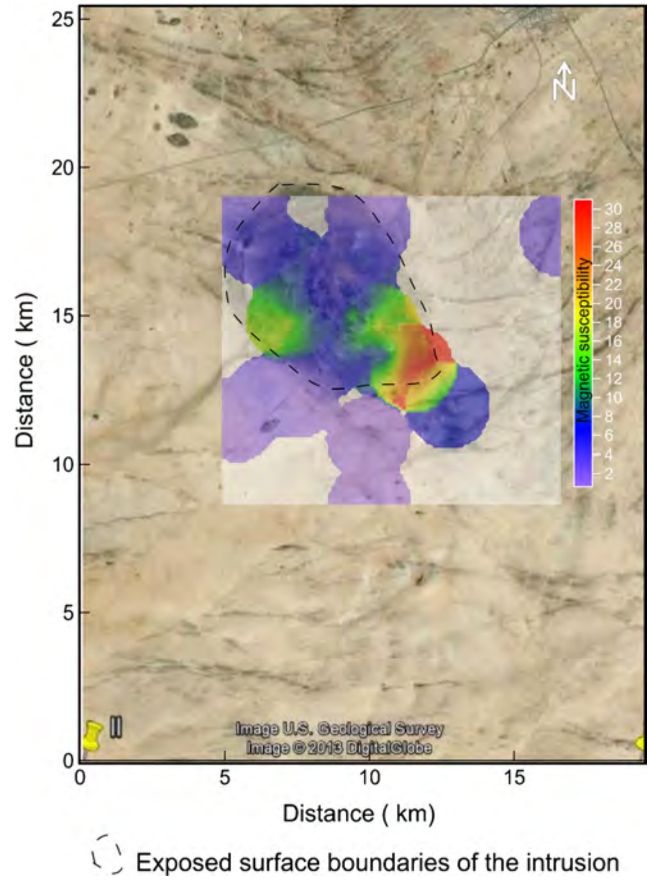

Fig. 13 Surface magnetic susceptibility map of Al Ji'lani intrusion. Low zones of susceptibility are observed at the northern and southern boundaries of the intrusion

analyses and inversion schemes succeeded in mapping basement topography, intrusions, and intra-sedimentary structures assuming clear and sharp physical boundaries. Magnetic methods are routinely used for this kind of studies (e.g. Middleton et al. 2004, Maes et al. 2008; Wilkes et al. 2011; Yang et al. 2011). The Al Ji'lani layered basic intrusion, Ad Dawadimdi district, Kingdom of Saudi Arabia, represents one of these interesting targets. The reduced-to-pole (RTP) magnetic intensity of the study area was calculated from the original total intensity aeromagnetic map of Saudi Arabia (Fig. 12). The RTP magnetic anomaly map (digitized to 87 × 100 data points) is characterized by a very distinctive oval anomalous zone centered over the exposed intrusion and extends beyond

Table 2 Statistical analyses of magnetic susceptibility readings (SI units) of some selected gabbroic layers

Easting(km)	Northing (km)	Sample No	Reading 1	Reading 2	Reading 3	Reading 4	Average
9.169	15.994	374	6.65	5.47	4.76	4.45	5.3325
9.785	15.268	375	5.79	5.25	8.6	9.14	7.195
9.448	15.016	357	23.3	16.2	0.53	0.51	10.135
8.911	15.268	356	22.3	18.9	11.6	16	17.2
9.670	14.743	366	8.75	7.17	9.47	8.48	8.4675
9.770	14.010	377	12.8	15.9	12.1	13	13.45
9.864	13.905	378	5.74	8.51	5.73	13	8.245
10.107	14.212	358	17.1	16.9	12.5	17.9	16.1
10.308	14.604	376	9.89	18.3	25.2	30.5	20.9725
10.601	13.653	359	10.9	7.3	8.27	10.4	9.2175

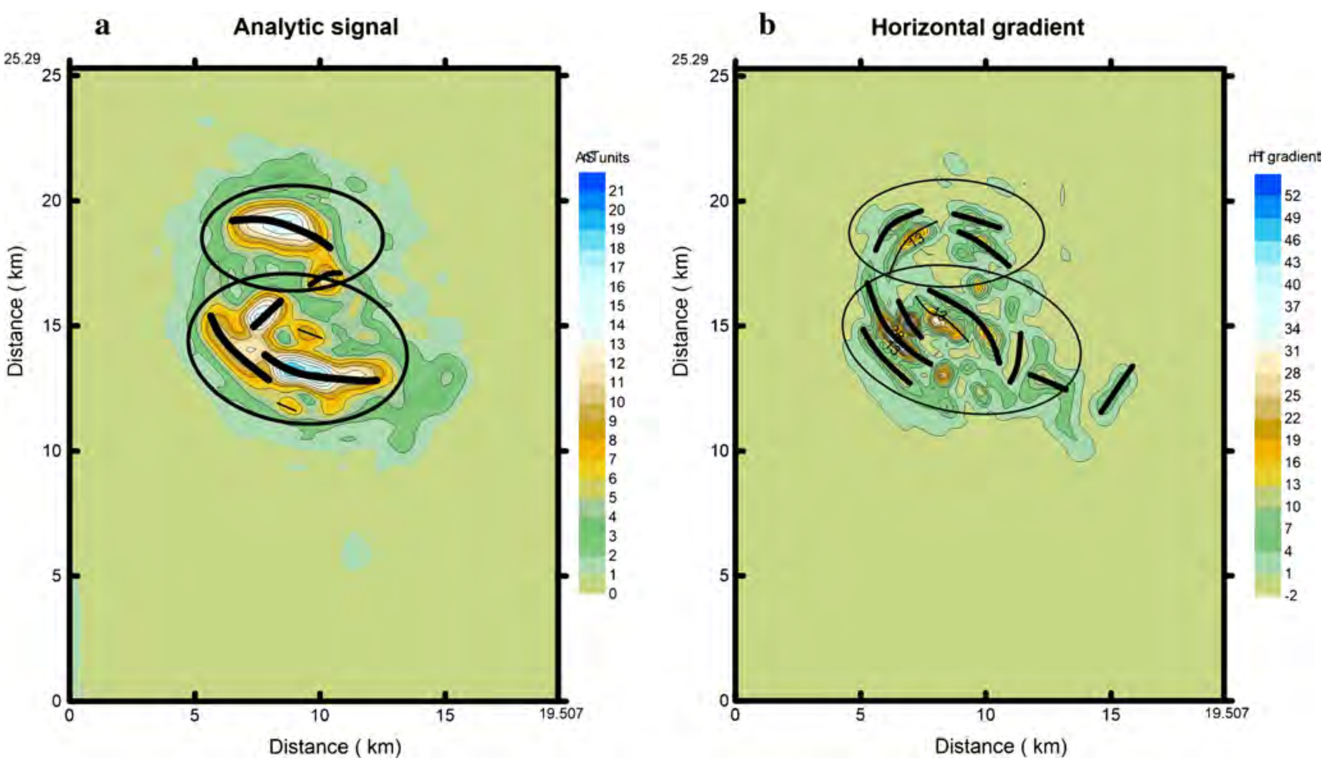

Fig. 14 Gradient analysis of Al Ji'lani intrusion. Analytic signal (**a**) and horizontal gradient (**b**)

Fig. 15 Tilt angle analysis of AL Ji'lani intrusion. Tilt angle with zero contour plotted. Depths to anomaly sources are posted as scaled colored circles

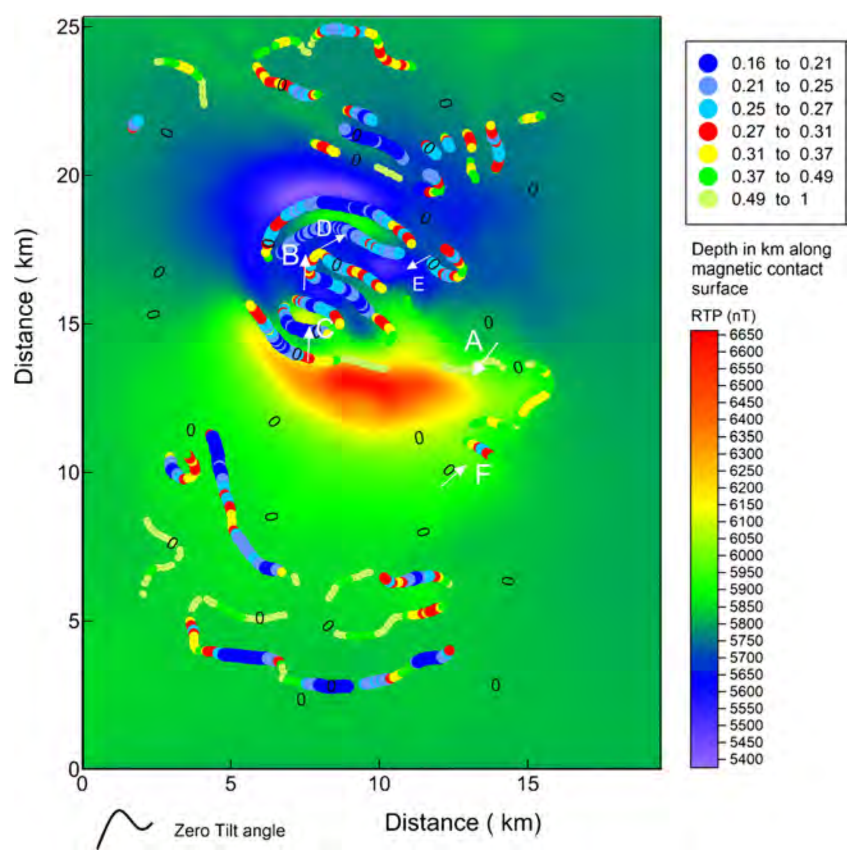

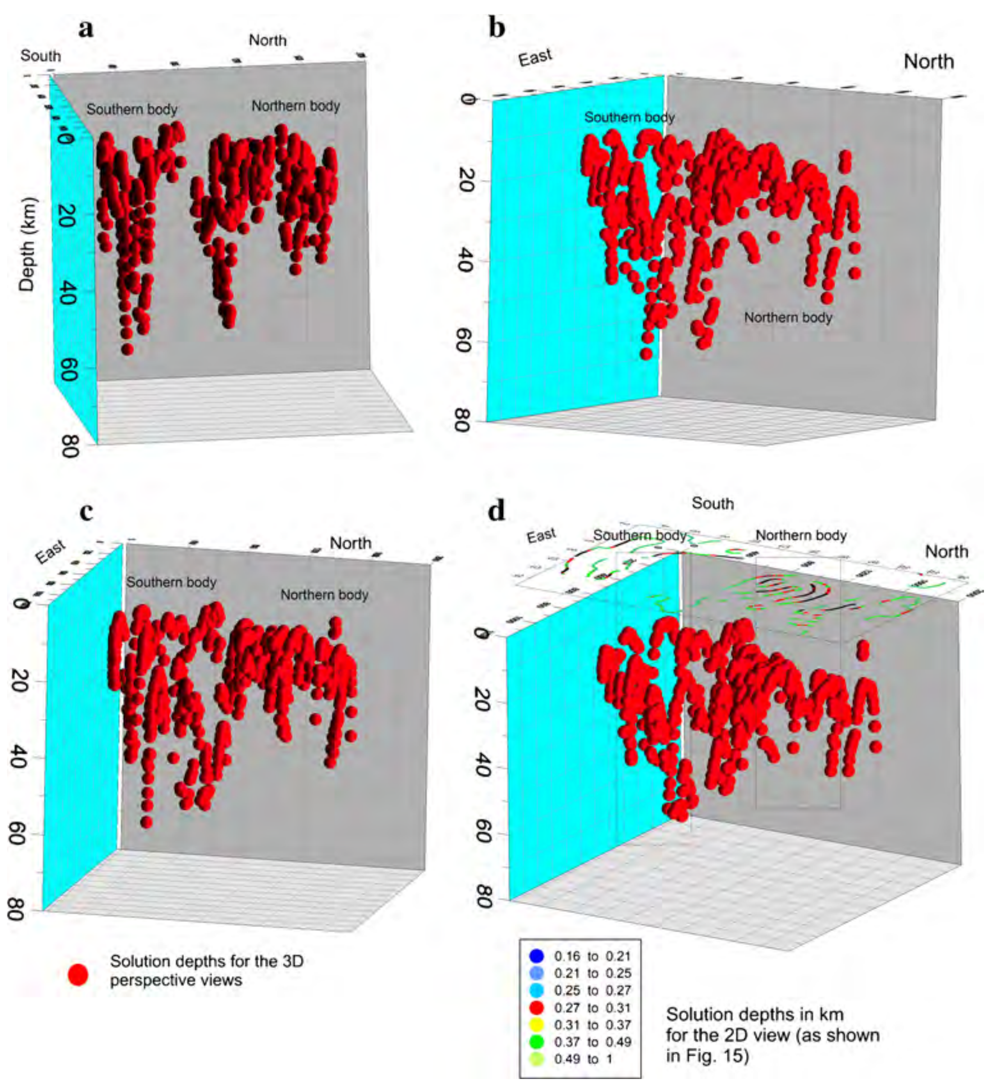

Fig. 16 Four different 3-D perspective views for the calculated depths using Tilt depth technique

the outlines of the surface exposure underneath the surrounding foliated granodiorite. The relief of the anomaly is about 1316 nT. Several minor anomalous features within the main body (anomalies B,C,D,E) less than 0.27 km in depth, (see section 3.2.1.) and outside the surface exposure (anomalies A and F) of depths range from 0.29 to 1.0 km, (see section 3.2.1.) can be recognized indicating strong variations in the magnetic properties within the same body. A general decrease in the amplitude of the anomaly is observed along a sample profile aa' running from SW to NE as shown in Fig. 12. A total number of 30 index rock samples were collected from the study area and the magnetic susceptibilities were measured using KT-10 magnetic susceptibility meter. Statistical analysis of the collected samples shows a relatively high average magnetic susceptibility (Table 1). The standard deviation of the values is found to be 6.40 and the average deviation is 4.47. The total average of the measured magnetic susceptibilities is 7.266.

A selective number of samples were extracted and statistically analyzed (Table 2). These samples were concentrated over the intrusive body. The results are used later for the 2D and 3D analysis and subsurface model construction. The analysis (Table 2) shows an average magnetic susceptibility of 11.6315 and a standard deviation of 5.06011. Most of the exposed intrusion rock types are gabbro, indicating high magnetic susceptibilities. Figure 13 shows the surface spatial distribution of the magnetic susceptibilities samples in the study area. A remarkable increase in the surface magnetic susceptibilities is observed running E-W crossing the lower half region of the intrusion. This indicates a possible lateral variation in

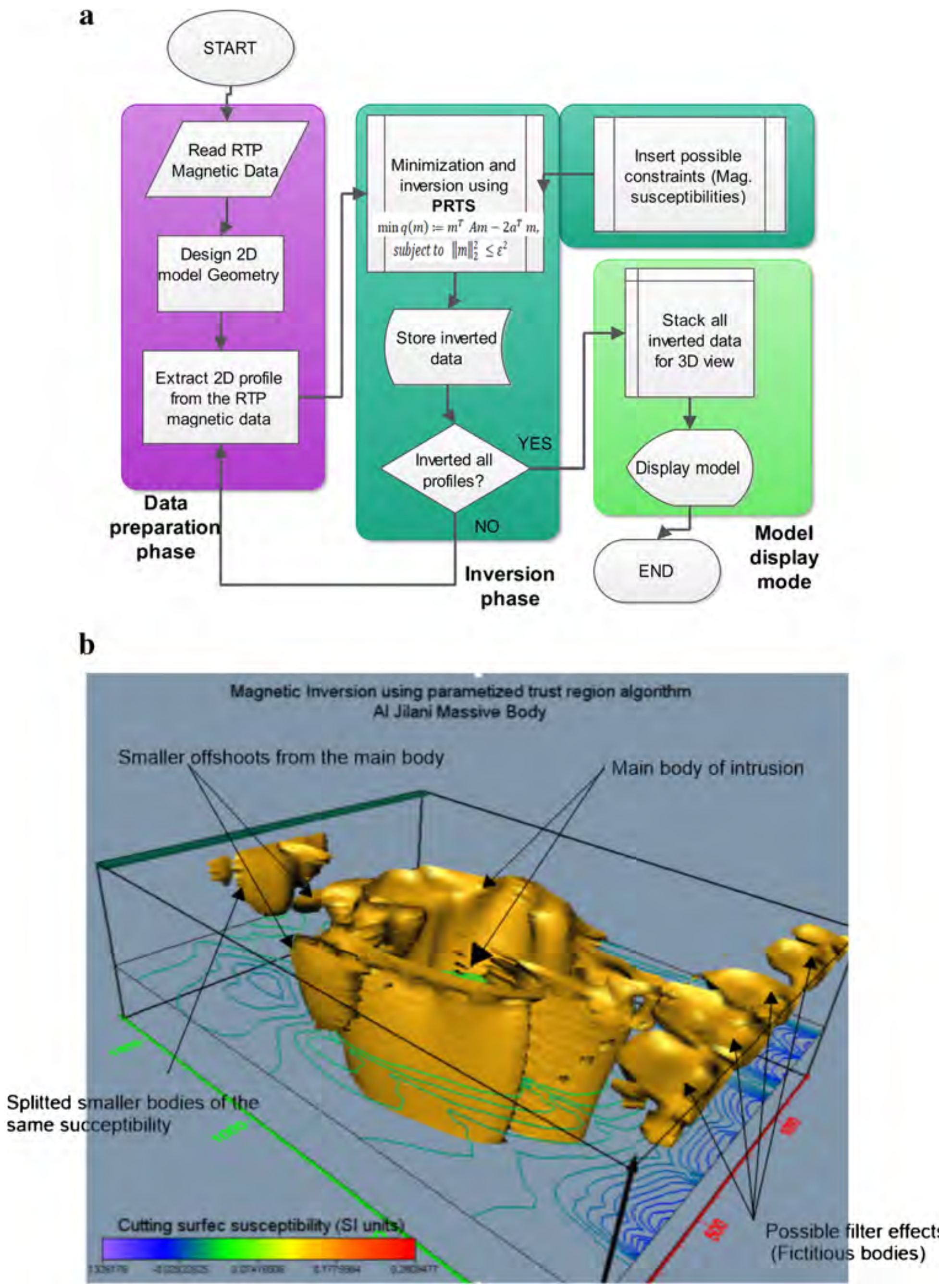

Fig. 17 **a** The workflow for the construction of the 3-D model. **b** Constraint 3-dimensional model of Al Ji'lani layered intrusion as resulted from regularized inversion using PTRS technique

rock types forming the intrusion. Generally, the magnetic susceptibility values are higher in the southern body (> 10 and up to 20.9 SI units) compared to the northern body (< 10 SI units). This is in agreement with the petrographic observations where olivine-bearing gabbros are widely distributed in the southern body (Fig. 7). In these rocks, olivine is oxidized and transformed into magnetite-orthopyroxene symplectites.

Quantitative analysis of magnetic data

The RTP map was filtered using Fourier transform to calculate directional gradients that enhance the structural features and lineaments in the area. The gradients T_x, T_y, T_z, T_{xx}, T_{yy}, T_{zz}, T_x, T_y, T_{xz}, *and* T_{yz} are calculated. Generally, the horizontal and vertical gradients (T_x, T_y, *and* T_z) are used for the visual enhancement of linear and curvilinear features in

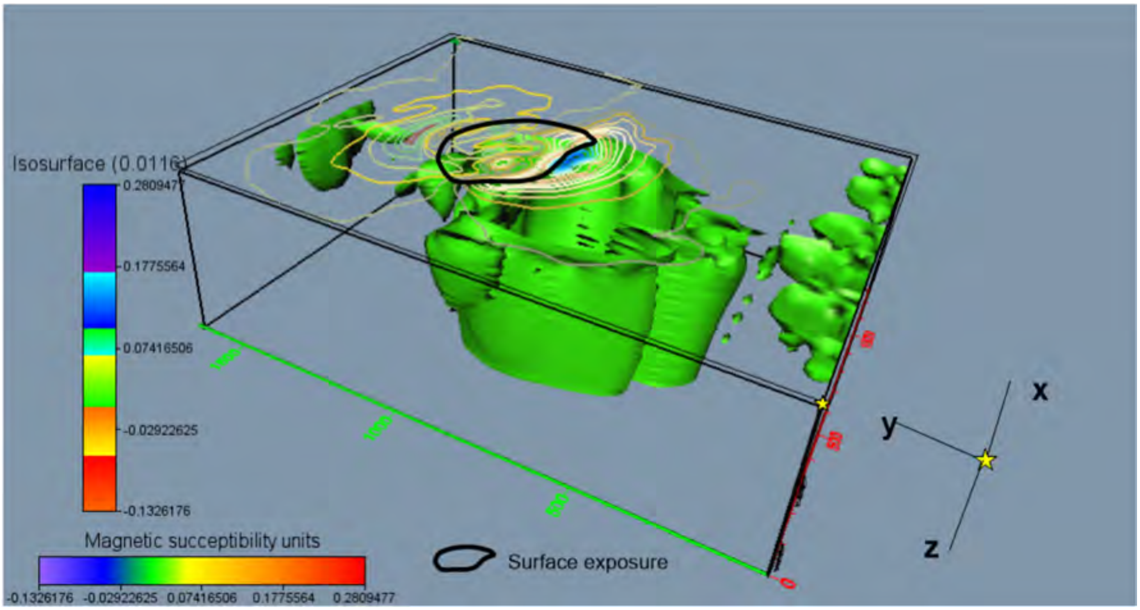

Fig. 18 Same as Fig. 17a but with posted surface exposure of the intrusion and RTP magnetic contours

the data. Both first and second degree gradients of the data $T_{RTP} = T(x,y)_{\mathrm{RTP}}$ can be computed. Here x direction represents the horizontal axis (Easting) and y direction the vertical axis (Northing) of the mapped data. The vertical gradients T_z *or* (dT/dz) are particularly useful in enhancing the lateral extensions of anomalous sources. The horizontal gradient, $h(x,y) = [d^2T/dx^2 + d^2T/dy^2]^{1/2}$, the total gradient, $a(x,y) = [d^2T/dx^2 + d^2T/dy^2 + d2T/dz2]1/2,$ the Tilt gradient, $t(x,y) = \arctan\ [df/dz.\ /\ h(x,y)]$, and the horizontal gradient of tilt gradient $s(x,y) = [d^2T/dx^2 + d^2T/dy^2]^{1/2}$ are proved to be useful operations that can used in visual interpretation of magnetic maps. They are used especially to produce the location of lateral contacts (edges) of different geological units. This property is used to estimate depth to contacts of the Al Ji'lani intrusion. Figure 14 shows the results of such analysis. Trend analysis of these maps shows two groups of curvilinear trends of magnetic boundaries within the target body, northern and southern groups of lineaments can be observed. Moreover, these boundaries are nearly concentric and probably vertical with high angle of dipping taking into account the sharp declination of the anomalous gradient fields. Lambolez (1968) reported that the magnetic pattern is due to a deep rooted-mafic body with a rather sharp and steeply dipping contact. The steep dipping contacts is in favor of the possibility of accumulation of ore minerals at depth. The intrusive body/bodies may be central massive block/blocks with two to three smaller offshoot bodies that differ in the magnetic susceptibilities.

Edge detection and depth to sources from magnetic data

For precise edge and depth enhancement, Salem and Williams (2007) proposed the Tilt-depth filter. The filter is applied directly on the Reduced to Pole magnetic anomaly maps. It assumes that the source body is a vertical contact model. The tilt angle is given as:

$$\theta = tan^{-1}\left(\frac{h}{z_c}\right) \qquad (1)$$

Where h is the distance from origin, z_c is the depth to top to the assumed contact model representing the edge boundaries, and θ in the Tilt angle in degrees.

The tilt angle filter is used to trace the border of bodies with different magnetic susceptibilities affecting the area and to calculate the depths to such bodies. The tilt amplitudes are bounded between -90^{o} and +90^{o} and correspond to a large dynamic range of amplitudes for anomalous sources at different depths (Oruc 2010). The value of the tilt angle is 0^{o} at the point $x = x_o$ above the edges of the contact. Therefore, the zero contours identify the horizontal location of the source. According to Salem and Williams (2007), the depth to source (z_o) is half the horizontal distance between +45^{o} contours of the tilt angle. Figure 15 shows the reduced to Pole anomaly map with calculated depths (colored posted circles) using the tilt-depth technique. The tilt boundaries corresponding to

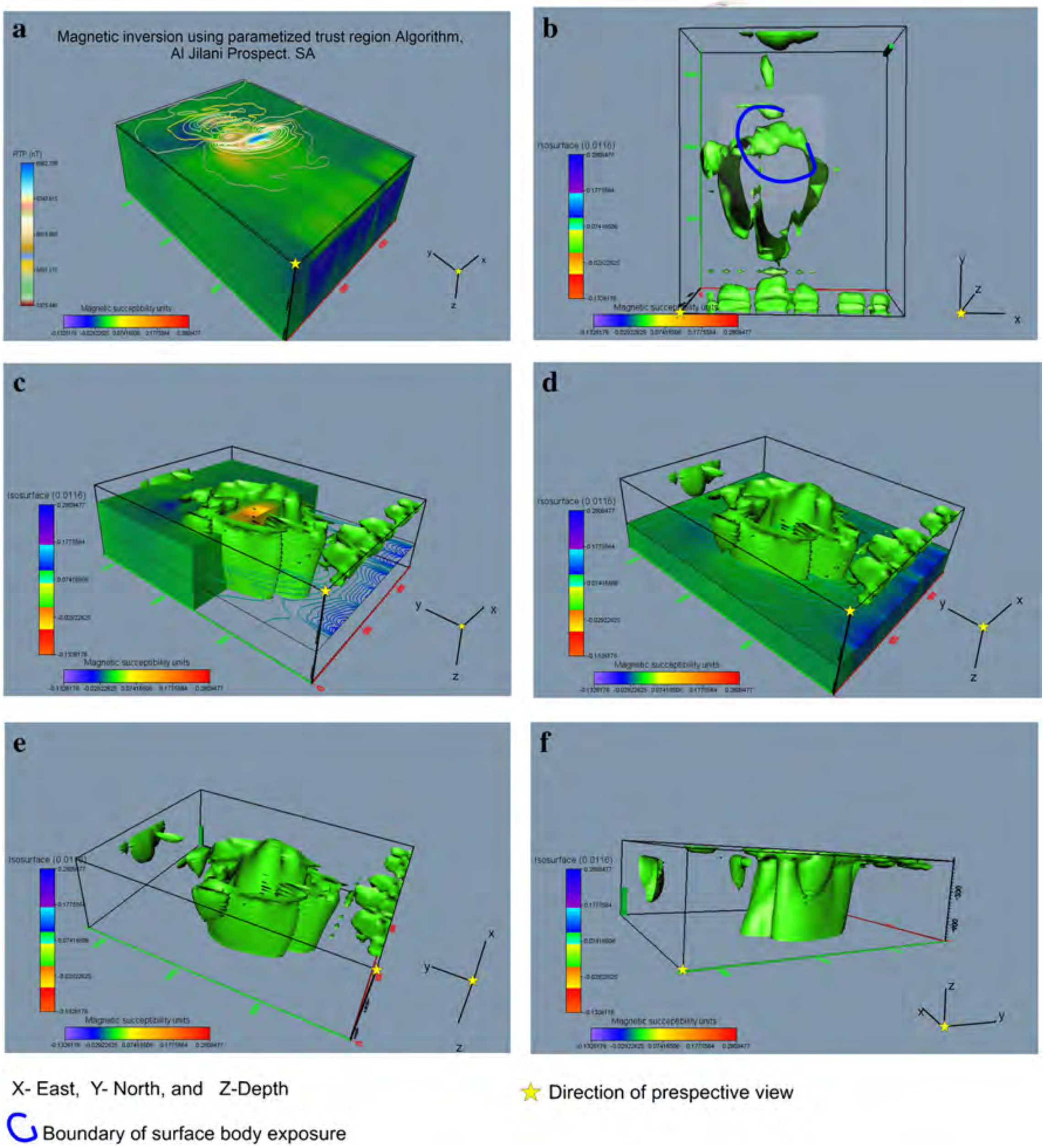

Fig. 19 Different perspective views to the model shown in Figs. 17 and 18

the zero contours indicate a clear subsurface variation in the magnetic susceptibilities and the diversity of rock units in the subsurface. The 3-dimensional perspective views for the area show these calculated depths with a clear splitting between two bodies can be recognized (Fig. 16a, b, c, d). Most of the anomalous field resulted from sharp and shallow contact surfaces (up to 1 km). The vertical contact model best fit the Al Ji'lani intrusive body.

Three-dimensional identification of Al Ji'lani intrusion by regularized inversion

Regularized inversion of potential field data is a pioneering class of strategies for modeling of subsurface structures and intrusions (Tikhonov and Arsenin 1977; Zhdanov 1993; Tezkan et al. 2000; Portniaguine and Zhdanov 2002; Fedi et al. 2005; Silva et al. 2007; Abdelazeem et al. 2007; Abdelazeem 2013; Blaschek et al. 2008, and Pășteka et al.

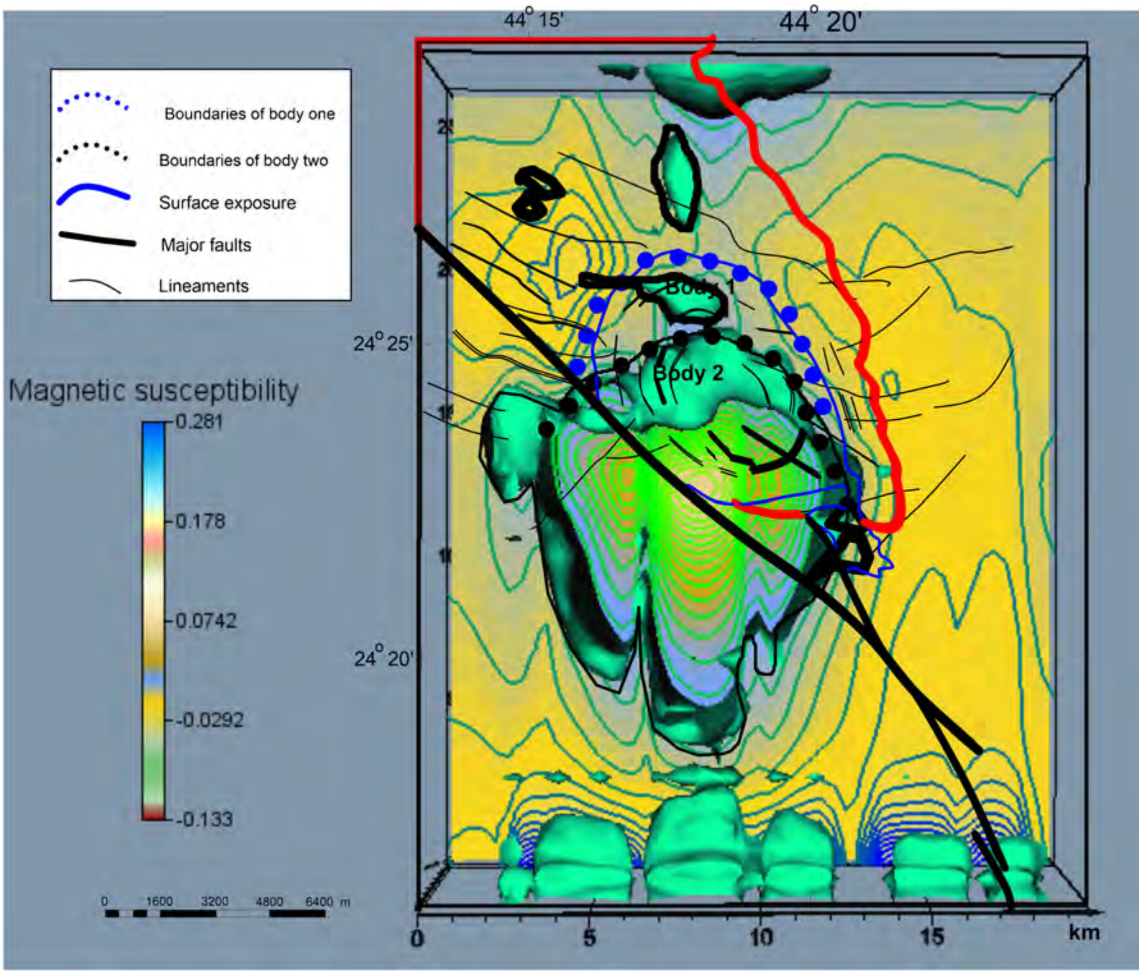

Fig. 20 Integrated interpretation of Al Ji'lani intrusion. Magnetic boundaries of the two bodies are marked

2012). Generally, the magnetic inverse problem is, intrinsically, non-unique and its numerical solution is unstable. This means that any small perturbation in the data (noise) causes large variation in the solution. Such noise, geophysically, is related to interfering models effects assuming the data is free from acquisition errors. Such a problem is a highly ill-posed one. Hence, a strong and stable strategy is required in order to end up with optimum solution. We applied regularization technique described by Abdelazeem (2013). The method is an extension to the traditional trust region approach combined with L-curve. The regularization parameter is deduced during inversion. The radius of the trust region is changed dynamically during iteration to improve the solution. Regularization depends here on choosing the parameter ε. The problem can be expressed simply as μ (A, a, ε) the so called trust-region sub-problem TRS (Fortin and Wolkowics 2004) as:

$$\mu(A, a, \varepsilon) \quad \min q(m) := m^T Am - 2a^T m, \quad subject\ to \quad \|m\|_2^2 \leq \varepsilon^2 \tag{2}$$

Where $A := G^T G$ is a M x M symmetric ($m > 2$), $a := G^T D$ is an m-vector. D is the observed RTP field. ε Is the trust-regions's fixed radius (positive scalar), and m is the m-vector of unknown magnetic susceptibilities of each block. All matrix and vector entries are real. For a detailed description of the technique, the reader can refer to Abdelazeem (op. cit.).

Abdelazeem (op. cit.) using unconstraint PTRS inversion showed that the two-dimensional test analysis of the Al Ji'lani suggests two near surface bodies extends to 273/249 units (4.14/3.8 km) (for body 2 to the south) and 149 units (2.27 km) (for body 1 to the north). In the present study, the algorithm applied again utilizing the available magnetic susceptibilities measured by the present authors as constraints and a priori information to the solution. This will give a plausible solution, increase the resolution and results in a more reliable bounded solution, i.e., implementation for priori information will improve the results quality and reduce uncertainty of result. This is mainly the advantage of adding

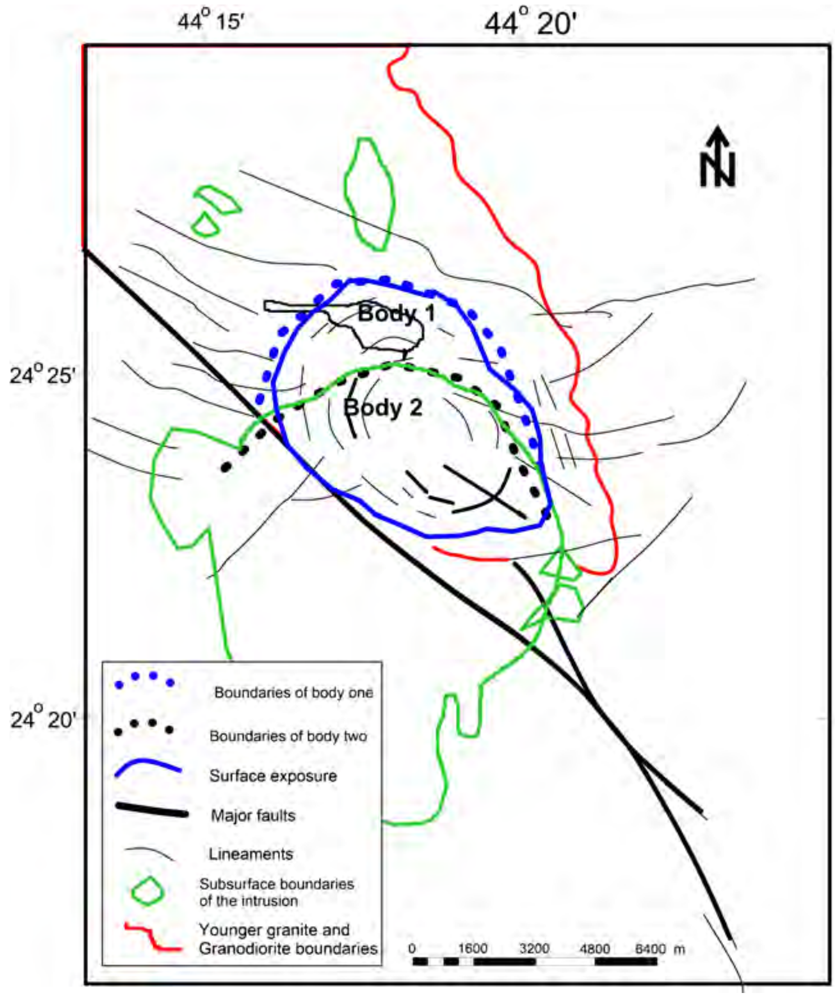

Fig. 21 Schematic diagram for the surface and subsurface structures as interpreted for Al Ji'lani prospect. Magnetic boundaries of the two bodies are marked

constraints to proposed solution and objective function used in the inversion.

In the constraint quasi 3-dimensional solution to the problem, the area is subdivided into 24 vertical sections (slices) running south north. The slice spacing is taken as 0.780 km meters. Each section comprises a model of 20 × 64 prismatic blocks (0.304 × 0.304 km) of unknown magnetic susceptibility m. This increases the accuracy with 3 prismatic blocks along each slice. The workflow for the construction of the 3-D model is shown in Fig. 17a. The final quasi 3-D model describing the iso-surface representing magnetic susceptibility 0.01163 SI units is shown in Figs. 17b and 18. Different perspective views to the same model are shown in Fig. 19a to f. The model consists of a main intrusion connected with smaller bodies to the west and north. All of these smaller bodies are in the subsurface. Other smaller intrusions can be observed north to the main intrusion (Fig. 17b). Sharp contact boundaries characterize the intrusion with a little dip inward, indicating a possible end at greater depths (more than 6 km) considering observed constraint susceptibility of ≥ 0.0116 SI units to the iso-surface presented which corresponds to the average susceptibility samples measured over the intrusion using KT-10 m. The calculated volume from the inverted model representing the Al Ji'lani layered intrusion is approximately 518.737 km^3 as calculated to a depth 6.0 km. The body could be extended to a deeper depth if a different proposed model geometry is adjusted.

Moreover, from the 3-dimensional analysis, the southern body surface exposure seems to be much smaller than the subsurface source body, which extends laterally and vertically. The Northern shallower body is now more resolved and confirmed to be of a very limited vertical extent. The above model is based on actual measured susceptibilities. The surface exposure of the Al Ji'lani body is narrower than the calculated mathematical model. This is true since we are modeling magnetic body not geologic surface. Based on our study, the southern magnetized body is extending in the subsurface to about 6 km to the south and southwest in the subsurface. This is clear as shown in Figs. 20 and 21. A probable nested pattern between the two bodies (body 1 to the north and main body 2 to the south) may cause the complicated anomaly pattern as shown in the original RTP map. Two zones can be identified and described by blue and black dashed lines in Fig. 21. The present model cube (45,619 blocks) extended to a depth of 6.0 km. A possible and expected deeper model may reveal the lower boundary of the extracted bodies. This requires a more detailed and resolved land total magnetic intensity survey.

Summary and conclusions

The results of the field, remote sensing, petrographic, and geophysical studies carried out on the Al Ji'lani layered mafic intrusion and its environ can be summarized as follows:

1. The intrusion is considered younger than the surrounding foliated granodiorite, i.e. post-orogenic, as it incorporates numerous masses from the foliated granodiorite.
2. The gabbroic rocks are fresh, undeformed, and characterized by the presence of kelyphytic coronas surrounding olivine when in contact with plagioclase, magnetite-orthopyroxene symplectites after olivine, and symplectites between plagioclase and magnetite/ilmenite. These textures can be explained in terms of interaction with late magmatic deuteric fluids and not to metamorphism as postulated in previous studies.
3. Joint processing of the aeromagnetic and magnetic susceptibility data using gradients and regularized inversion techniques indicate that the Al Ji'lani layered mafic body is a multiple intrusion of a northern shallow body and a more deeper southern body. The intrusion extends in the subsurface to the south and southwest, beyond the outlines of the surface exposure of the intrusion, underneath the foliated granodiorite. Al Ji'lani layered intrusion is approximately 518.7 km^3 as calculated to 6.0 km depth. The body could be extended to a deeper depth if a different proposed model geometry is adjusted. The surface area of the exposed body is only 42.39 km^2.

In the light of these findings, it is concluded that the Al Ji'lani layered intrusion is post-orogenic, younger than the foliated granodiorite and older than the younger granite. The intrusion possesses numerous magnetic anomalies within the area of surface exposure and can be considered potential sites of mineralization. The Samrah Prospect sulfide-bearing quartz veins with high silver content (653 g/t), 5.12% Zn, and 1.64% Pb are hosted in a shear zone traversing an offshoot from the layered gabbro to the SE of the intrusion. The shear zone should be followed to the west where the intrusion extends for a distance of about 10 km in the subsurface to the southwest of the exposed part of the intrusion.

Acknowledgements This work was funded by the Deanship of Scientific research (DSR), King Abdulaziz University, Jeddah, under grant no. (145-331-D1435). The authors, therefore, acknowledge with thanks DSR technical and financial support. Many thanks to Dr. Maha Abdelazeem (National Research Institute for Astronomy and Geophysics, Egypt, NRIAG) for her help in 3D inversion of the data using PTRS algorithm and code justification.

References

Abdel Wahed, M Zoheir B, Hamimi, Z and El-Selwi, KH (2006) Tectonic evolution of the Archean- Neoproterozoic Basement Complex of Dhi-Al Bayda District, Republic of Yemen, Intern. Conf. Geol. The Arab World, Cairo University, Egypt, pp 135–146

Abdelazeem M (2013) Regularizing ill-posed magnetic problems using a parameterized trust-region sub-problem. Contributions to geophysics and geodesy. 43/2:99–123

Abdelazeem M, Sweilam NH, Gobashy M, Nagy AMA (2007) Two-dimensional gravity inverse problem using adaptive pruning L-curve technique. Bull Fac Sci, Cairo Univ 75(A):93–115

Abrams MJ, Brown D, Lepley L, Sadowski R (1983) Remote sensing for porphyry copper deposits in southern Arizona. Econ Geol 78(4): 591–604. https://doi.org/10.2113/gsecongeo.78.4.591

Akaad MK (1996) Rock succession of the basement, an autobiography and assessment. Geol Surv Egypt 71:1–87

Al Shanti A (1974) Al Ji'lani layered basic intrusion, ad Dawadimi District, Kingdom of Saudi Arabia, directorate general of mineral resources, Jiddah. Miner Resour 12:1–45

Al Shanti AMS, Mitchell AHG (1976) Late Precambrian subduction and collision in the Al Amar-Idsas region, Arabian shield, Kingdom of Saudi Arabia. Tectonophysics 30:14–47

Ambler EP, Ashley PM (1977) Vermicular orthopyroxene–magnetite symplectites from the Wateranga layered mafic intrusion, Queensland, Australia. Lithos 10(3):163–172. https://doi.org/10.1016/0024-4937(77)90044-5

Assiri A, Alsaleh A, Mousa H (2008) Exploration of hydrothermal alteration zones using ASTER imagery: a case study of Nuqrah area, Saudi Arabia. Asian J Earth Sci 1:77–82

Bakor AR, Gass IG, Neary C (1976) Jabal Al Wask, Northeast Saudi Arabia, an Eocambrian back-arc ophiolite, earth and planet. Sci Lett 30:1–9

Barton M, Gaans CV (1988) Formation of orthopyroxene–Fe-Ti oxide symplectites in Precambrian intrusive Rogaland, southwestern Norway. Am Mineral 73:1046–1059

Basta EZ, Girgis MH (1969) Petrological, mineralogical and geochemical studies on magnetite-ilmenite-apatite ore (nelsonite) from Kolminab, south Eastern Desert, Egypt, the proceed. Egypt. Acad Sci 22:235–440

Blaschek R, Hordt A, Kemna A (2008) A new sensitivity-controlled focusing regularization scheme for the inversion of induced polarization data based on the minimum gradient support. Geophysics 73: 45–54

Bokhari FY, Kramers JD (1981) Island arc character and later Precambrian age of volcanics at shwas, Saudi Arabia, geochemical and Sr-Rb isotopic evidence. Earth Planet Sci Lett 54(3):409–422. https://doi.org/10.1016/0012-821X(81)90057-1

Calvez JY, Alsac C, Delfour J, Kemp J and Pellaton C (1983) Geological evolution of western, central and eastern part of the Northern Precambrian Shield, Kingdom of Saudi Arabia, Saudi Arabia Deputy Ministry for Mineral Resources, Open-File Report BRGM-OF-17

Chen CM (2000) Comparison of principal component analysis and minimum noise fraction transformation for reducing the dimensionality of hyperspectral imagery. Geogr Res 33:163–178

Chevremont P (1983) Bibliographic review of platinum-group mineralization in the world and the possibility of such mineralization within the ultramafic-mafic complexes in Saudi Arabia: Saudi Arabian Deputy Ministry for mineral Resources Technical Record BRGM-TR-03-3:1–62

Claeson DT (1998) Coronas, reaction rims, symplectites and emplacement depth of the Rymmen gabbro, Transscandinavian igneous belt, southern Sweden. Mineral Mag 62(6):743–757. https://doi.org/10.1180/002646198548133

Cloeman RG, Ghent ED, Fleck RJ (1977) The Jabal Shay'i gabbro in Southwest Saudi Arabia, with a section on geophysical studies by Griscom. A Saudi Arabian Dir Gen Miner Resour Bull 17:1–46

Coleman RG, Brown GF, Keith TEC (1972) Layered gabbros in Southwest Saudi Arabia, U.S. Geol Surv Prof 900:143–150

Collenette P and Grainger DJ (1994) Mineral resources of Saudi Arabia, D G M R special publication. 2:1–322

Delfour J (1981) Geologic, tectonic and metallogenic evolution of the northern part of the Precambrian Arabian shield (kingdom of Saudi Arabia). Bull Bur Rech Min (deuxiem serie) 1-2. Section 11:1980–1981

Delfour J Dhellamme R Elsass P Vaslet D Brosse JM Le Nindie YM and Dottin O (1982) Explanatory notes to the map of the Ad Dawadimi Quadrangle, Sheet 24G, Kingdom of Saudi Arabia, Ministry of Petroleum and Mineral Resources, Deputy Ministry Miner Resour 1–36

Efimov AA, Malitch KN (2012) Magnetite-orthopyroxene symplectites in gabbros of the Urals: a structural track of olivine oxidation. Geology of Ore Deposits 54(7): 531–539 (translated from Zapiski Rossiiskogo Mineralogicheskogo Obshchestva 2010 139(5):18–28

El Ramly MF and Hermina MH (1978a) Geologic map of the Qena quadrangle, Egypt, scale 1: 500,000, published in cooperation with U.S. Geological Survey under the auspices of the U.S. Agency for International Development (USAID)

El Ramly MF and Hermina MH (1978b) Geologic map of the Aswan quadrangle, Egypt, scale 1: 500,000, published in cooperation with U.S. Geological Survey under the auspices of the U.S. Agency for International Development (USAID)

El Tokhi M, El Muslem A (2002) Fluid inclusions in the gold-bearing quartz veins at Um Rus area, Eastern Desert, Egypt. Chin J Geochem 2:131–139

Fedi M, Hansen PC, Paoletti V (2005) Analysis of depth resolution in potential-field inversion. Geophysics 70:1–11

Fleck RJ, Greenwood WR, Hadley DG, Andreson RE and Schmidt DL (1980) Rubidium-Strontium geochronology and plate tectonic evolution of the southern part of the Arabian Shield, US. Geological survey, Professional Paper 1131

Fortin C, Wolkowics H (2004) The trust region sub-problem and semidefinite programming. Optim Methods Softw 19:41–67 (special issue dedicated to Jochem Zowes 60th birthday, guest editors: Florian Jarre and Michal Kocvara)

Frisch W, Al Shanti A (1977) Ophiolite belts and the collision of island arcs in the Arabian shield. Tectonophysics 43(3-4):293–306. https://doi.org/10.1016/0040-1951(77)90121-4

Gad S, Kusky TM (2007) ASTER spectral ratioing for lithological mapping in the Arabian-Nubian shield, the Neoproterozoic Wadi kid area, Sinai, Egypt. Gondwana Res 11(3):326–335. https://doi.org/10.1016/j.gr.2006.02.010

Garson MS, Shalaby IM (1976) Precambrian-Lower Paleozoic plate tectonics and metallogenesis in the Red Sea region, Geol. Ass. Canada. Spec Paper 14:573–596

Gass IG (1977) The evolution of the pan-African crystalline basement in NE Africa and Arabia. Geol Soc Lond J 134:129–138

Gass IG, Smewing JD (1981) Ophiolite-obducted oceanic lithosphere. In: Emiliani C (ed) The sea–the oceanic lithosphere, vol 7. John Wiley and Sons, New York, pp 339–362

Genna A, Nehlig P, Le Goff E, Guerro, Shanti M (2002) Proterozoic tectonism of the Arabian shield. Precamb Res 117(1-2):21–40. https://doi.org/10.1016/S0301-9268(02)00061-X

Gomez G, Delacourt C, Allemand P, Ledru P, Wackerle R (2005) Using ASTER remote sensing data set for geological mapping, in Namibia. Phys Chem Earth 30(2005):97–108. https://doi.org/10.1016/j.pce.2004.08.042

Greenwood WR, Hadley DG, Anderson RF, Fleck RJ, Schmidt DL (1976) Late Proterozoic cratonization in Southwestern Saudi Arabia. R Soc Lond Phil Trans Ser 280:517–527

Harbi HM (2004) Genesis of gold mineralization at Zalm area, Central Saudi Arabia, Kingdom of Saudi Arabia, 6th International Conf. on Geochemistry, Alex. Univ., Egypt, 143–160

Harbi HM, Hassanen MA Eldougdoug AA and Sahal MSA (2003) Geological and geochemical studies on some gold occurrences in Zalm Quadrangle, Western Afif Terrane, Arabian Shield, Saudi Arabia, The Final Report for Project No. 421/203, King Abdulaziz University, Institute of Research and Consultation, Jeddah, Saudi Arabia. 1–69

Harbi HM, Hassanen MA, Eldougdoug AA, and Al-Filali IY (2006) Economic potentiality and petrogenetic evolution of the mafic-ultramafic rocks in the Wadi Khamal area, northwestern Arabian shield, Saudi Arabia, final report for project no. 203/424, king Abdulaziz university, Institute of Research and Consultation, Jeddah, Saudi Arabia. 1-85

Hassan MA and Hashad AH (1990) Precambrian of Egypt, In: The Geology of Egypt (Edited by Rushdi Said), A. A. Balkema /Rotterdam /Brookfield

Helmy HM, Mogessie A (2001) Gabbro Akarem, Eastern Desert, Egypt: cu-Ni-PGE mineralization in a concentrically zoned mafic-ultramafic complex. Mineral Deposita 36(1):58–71. https://doi.org/10.1007/s001260050286

Hussein AA (1990) Mineral deposits, in: the geology of Egypt (edited by Rushdi said), A.A. Balkema /Rotterdam /Brookfield

Jackson NJ (1985) Petrogenesis and evolution of the Arabian felsic plutonic rocks and associated mineralization of Kingdom of Saudi Arabia, DMMR, Mineral Resources Bull., No.29.(Eds. Drysdall, A.R., Ramsay, C.R., and Stoeser, D.B.). 47-62

Johnson PR (1999) Tectonic development of the Arabian Shield: an overview, U.S. Geological Survey Saudi Arabian Mission, IUGS/UNESCO Deposit modeling workshop, Jeddah, Saudi Arabia, Nov. 2009

Johnson P and Kattan FH (2012) The geology of the Saudi Arabian shield. King Fahad National Library Catalouge In Publication Data, Saudi Arabia 1–479

Johnson PR, Andresen A, Collins AS, Fowler AR, Fritz H, Ghebrab W, Kusky T, Stern RJ (2011) Late Cryogenian-Ediacaran history of the Arabian-Nubian shield: a review of depositional, plutonic, structural, and tectonic event in the closing stages of the northern east African Orogen. J Afr Earth Sci 61(3):167–232. https://doi.org/10.1016/j.jafrearsci.2011.07.003

Kemp J, Pellaton C, Calvez JY (1982) Cycle in the orogenic evolution of the Precambrian shield in part of northwestern Saudi Arabia. Dir Gen Miner Resour Professional Paper 1:27–41

Kroner A (1985) Ophiolites and evolution of the tectonic boundaries in the late Proterozoic Arabian-Nubian shield of northeastern Africa and Arabia. Precamb Res 27(1-3):277–300. https://doi.org/10.1016/0301-9268(85)90016-6

Lambolez B (1968) Aeromagnetic and scintillometric survey, 1966–1967, report on starting operations, Saudi Arabian Gen. Mineral resources, Open-File-Report

Maes SM, Ferré EC, Tikoff B, Brown PE, Marsh JS (2008) Magnetostratigraphy of a mafic layered sill: a key to the Karoo volcanics plumbing system. J Volcanol Geotherm Res 172(1-2):75–92. https://doi.org/10.1016/j.jvolgeores.2005.07.038

Mars JC, Rowan LC (2006) Regional mapping of phyllic- and argillic-altered rocks in the Zagros magmatic arc, Iran, using advanced Spaceborne thermal emission and reflection radiometer (ASTER) data and logical operator algorithms. Geosphere 2(3):161–186. https://doi.org/10.1130/GES00044.1

Mather PM (1987) Computer processing of remotely sensed images. John Wiley and Sons, Chechester, pp 1–328

Middleton RS, Borradaile GJ, Baker D, Lucas K (2004) Proterozoic diabase sills of northern Ontario: magnetic properties and history. J Geophys Res 109(B2). https://doi.org/10.1029/2003JB002581

Mouhssine W, Taj-Eddine K, Laftouhi N (2013) ASTER VNIR & SWIR band enhancement for lithological mapping a case study of the Azegour area (western high atlas, Morocco). J Environ Earth Sci 3(12):2013

Nehlig P, Genna A, Asfirane F (2002) A review of the Pan-African evolution of the Arabian shield. Geo Arabia 7(1):103–124

Oruc B (2010) Edge detection and depth estimation using a tilt angle map from gravity gradient data of Kozakli-Central Anatolia region, Turkey. Pure Appl Geophys 168:769–1780

Păsteka R, Karcol R, Kusnir'ak D, Mojzes A (2012) REGCONT, A Matlab based program for stable downward continuation of geophysical potential fields using Tikhonov regularization. Computer and Geosciences 49:278–289

Portniaguine O, Zhdanov MS (2002) 3-D magnetic inversion with data compression and image focusing. Geophysics 67(5):1532–1541. https://doi.org/10.1190/1.1512749

Pour AB, Hashim M (2011) Spectral transformation of ASTER data and the discrimination of hydrothermal alteration minerals in a semi-arid region, SE Iran. Int J Phys Sci 6(8):2037–2059

Rowan LC, Mars JC (2003) Lithologic mapping in the mountain pass, California area using advanced Spaceborne thermal emission and reflection radiometer (ASTER) data. Remote Sens Environ 84(3): 350–366. https://doi.org/10.1016/S0034-4257(02)00127-X

Rowan LC, Hook SJ, Abrams MJ, Mars JC (2003) Mapping hydrothermally altered rocks at cuprite, Nevada, using the advanced Spaceborne thermal emission and reflection radiometer (ASTER). A new satellite-imaging system. Econ Geol 98(5):1019–1027. https://doi.org/10.2113/gsecongeo.98.5.1019

Sabins F (1997) Remote sensing principles and interpretation. 3rd ed. pp1-494

Salem A, Williams S (2007) Tilt-depth method: a simple depth estimation method using first-order magnetic derivatives. The. Lead Edge 26(12):1502–1505. https://doi.org/10.1190/1.2821934

San Miguel-Ayanz J, Biging GS (1996) An iterative classification approach for mapping natural resources from satellite imagery. Int J Remote Sens 17(5):957–981. https://doi.org/10.1080/01431169608949058

Schmidt DL, Hadley DG, Greenwood WR, Gonzalez L, Coleman RG, Brown GF (1973) Stratigraphy and tectonism of the southern part of the Precambrian shield of Saudi Arabia. Saudi Arabia Directorate Gen Miner Resour Bull 8:1–13

Silva JBC, Oliveira FS, Barbosa VCF, Velho HFC (2007) Apparent density mapping using entropic regularization. Geophysics 72(4):151–160

Stacey JS, Hedge CE (1984) Geochronology and isotopic evidence for early Proterozoic continental crust in eastern Arabian shield. Geology 12(5):310–313.

Stacey JS, Stoeser DB (1983) Distribution of oceanic and continental lead in the Arabian-Nubian shield. Contr Miner Petrol 48:91–105

Stacey JS, Delevaux MH, Gramllich JW, Done BR, Robert RJ (1980) A lead isotopic study of mineralization in the Arabian shield. Contr Miner Petrol 74:157–188

Stoeser DB and Camp VE (1984) Pan African microplate accretion of the Arabian shield, Saudi Arabian deputy for mineral resources, technical record USGS TR-04-17

Surour Adel A, Ahmed AH and Harbi HM (2016) Mineral chemistry as a tool for understanding the petrogenesis of Cryogenian (arc-related) – Ediacaran (post-collisional) gabbros in the western Arabian shield of Saudi Arabia. https://doi.org/10.1007/s00531-016-1371-7.

Takla MA, Basta EZ, Fawzi E (1981) Characterization of the older and younger gabbros of Egypt, Delta. J Sci 5:279–314

Takla MA, Eldougdoug AA, Rasmy AH, Gad MA, Eltabal HK (1990) Origin of um Eleiga gold mineralization. South Eastern Desert, Egypt, Egyptian Mineralogist 2:3–20

Takla MA, Eldougdoug AA, Gad MA, Rasmy AH and Eltabal HK (1997) Gold-bearing quartz veins in mafic and ultramafic rocks, Hutite and um Tenedba, south Eastern Desert, Egypt. Annals Geol Surv Egypt XX 411–432

Tawfik TM (1981) Geology of Dirbat Well area, Red Sea Hills, Sudan. Unpublished M.Sc., Faculty of Science, Cairo University 1–40

Tezkan B, Hoerdt A, Gobashy M (2000) Two dimensional radiomagnetotelluric investigation of industrial and domestic waste sites in Germany. J Appl Geophys 44(2-3):237–256. https://doi.org/10.1016/S0926-9851(99)00014-2

Theobold PK Jr (1966) Geology of Samrah and vicinity, U.S. Geol Surv Tech Lett 42:1–24

Tikhonov AN and Arsenin VY (1977) Solutions of ill-posed problems. V. H. Winston and Sons

Vail JR (1983) Pan African crustal accretion in northeast Africa. J African Earth Sci 1:285–294

Wilkes PG, Timms N, Corbel S and Horowitz FG (2011) Using gravity and magnetic methods with geomorphology and geology for basement and structural studies to assist geothermal applications in the Perth Basin. Australian Geothermal Energy Conference

Yang X, Scuderi L, Liu T, Paillou P, Li H, Dong J, Zhu B, Jiang W, Jochems A, Weissmann G (2011) Formation of the highest sand dunes on earth. Geomorphology 135(1-2):108–116. https://doi.org/10.1016/j.geomorph.2011.08.008

Zhdanov MS (1993) Regularization in inversion theory: tutorial, Colorado School of mines